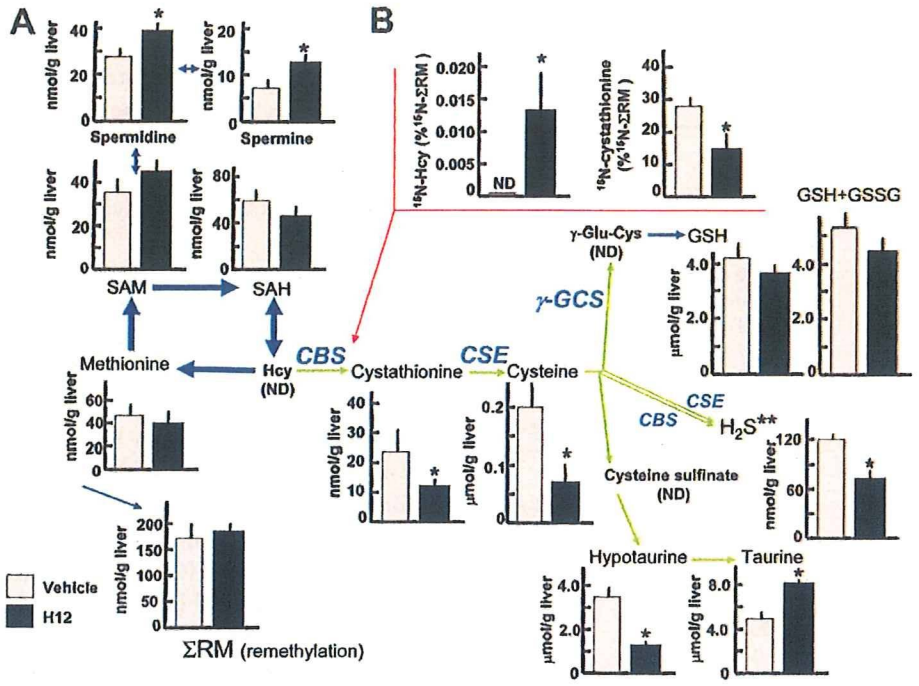

Fig. 2. Metabolomic comparison of sulfur-containing amino acids and their derivatives between the heme-overloaded and vehicle-treated livers of mice. (A) Differences in hepatic contents of the metabolites between the control and hemin-treated mice. H12: treatment with hemin at 12 hours before sampling the liver. Note decreases in transsulfuration metabolites. (B) *In vivo* pulse-chase analysis indicating conversion rates of ^{15}N-methionine into ^{15}N-homocysteine (Hcy) and ^{15}N-cystathionine in livers between the groups. The amounts of the downstream metabolites were measured at 30 minutes after the methionine administration. The data in B were normalized by total amounts of metabolites in remethylation cycle (^{15}N-methionine + ^{15}N-SAM + ^{15}N-SAH + ^{15}N-Hcy = ΣRM) at 30 minutes. ND, not detected. Data indicate mean ± SE of six to eight separate experiments for each group. *$P < 0.05$ versus the vehicle-treated group.

acids led us to reveal unique physiological actions of this gas on CBS *in vivo* that are not shared with NO. The current study suggested that stress-inducible CO targets CBS and thereby reduces H_2S significantly to stimulate biliary HCO_3^- excretion that could benefit detoxification processes. Conversely, such a property of stress-inducible CO might jeopardize anti-oxidative defense systems through an overflow of homocysteine or through a shortage of GSH. Under current experimental conditions, however, such a risk seemed little, if any, so far as judged from maintenance of GSH and adenosine triphosphate so far. This appears to result from large difference in amino acid pools between methionine (nmol/g) and thiols including cysteine and GSH (μmol/g). Furthermore, cysteine could be supplied through its uptake from extracellular space by mechanisms involving Nrf2, the transcriptional factor activated in response to oxidative stress or electrophiles such as heme.[28,29] By contrast, the amounts of sulfur-containing amino acids consumed to generate H_2S seems relatively smaller than that for synthesizing GSH or hypotaurine, as judged from quantitative information collected by metabolome analysis. Because CBS not only limits synthesis of cystathionine from homocysteine but also directly suppresses H_2S generation from cysteine, the inhibitory effects of CO on the enzyme could dictate largely on the action of H_2S in the liver, causing a stimulatory effect on bile excretion. Considering recent studies suggesting vasodilatory effects of H_2S,[26,30] suppression of CBS-derived H_2S by stress-inducible CO might trigger vasoconstriction, but such vasoactive responses did not occur so far as judged from choleretic response of the basal bile flow that is highly dictated by microvascular perfusion. This might result from the fact that stress-inducible CO itself has the ability to maintain the basal microvascular perfusion through multiple vasodilatory mechanisms involving activation of cyclic guanosine monophosphate and modulation of cytochrome P450–derived vasoconstrictors.[6,20,31]

Although the inhibitory action of stress-inducible CO on the transsulfuration pathway has first been shown in the heme-overloading detoxification model of mice in the current study, a similar event occurred in acetaminophen-induced acute liver injury model of mice in which CO was overproduced through degradation of cytochrome P450–derived heme.[5,18] Our previous study in rats suggested that another HO-derived product bilirubin but not CO

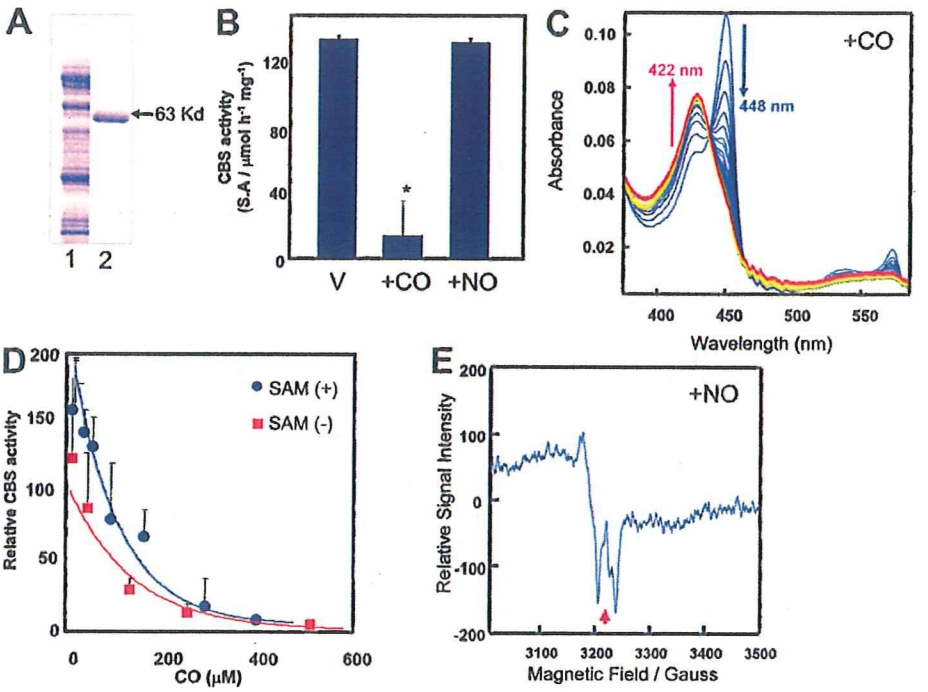

Fig. 3. Effects of CO and NO on the activity and structure of the prosthetic heme of rat recombinant full-length CBS. (A) Sodium dodecyl sulfate polyacrylamide gel electrophoresis for purification of rat recombinant CBS. Lane 1, crude extract; lane 2, purified CBS. (B) Effects of CO and NO on the Fe(II)-CBS activity under optimal substrate conditions at pH 7.4. CO but not NO (100 μM) significantly attenuated the activities of the ferrous enzyme. Data indicate mean ± SE of four experiments. The activities were measured by determining conversion of homocysteine and serine to cystathionine. *$P < 0.05$ versus the group treated with vehicle (V). The concentration of CBS-heme was 10 μM. (C) Stopped-flow visible spectrophotometry for Fe(II)-CBS to examine temporal transitional changes after mixing with CO. Data exhibited a drop at 449 nm and a reciprocal elevation at 422 nm, demonstrating stabilization of the 6-coordinated CO-Fe(II)-histidine complex. K_{obs} = 0.638/second. (D) Effects of CO on the CBS activities in the presence or absence of S-adenosyl methionine (SAM), the allosteric activator of the enzyme. (E) Electron spin resonance spectrometry indicating 5-coordinated NO-Fe(II) complex of the CBS-heme. Arrow: *g*-value = 2.008.

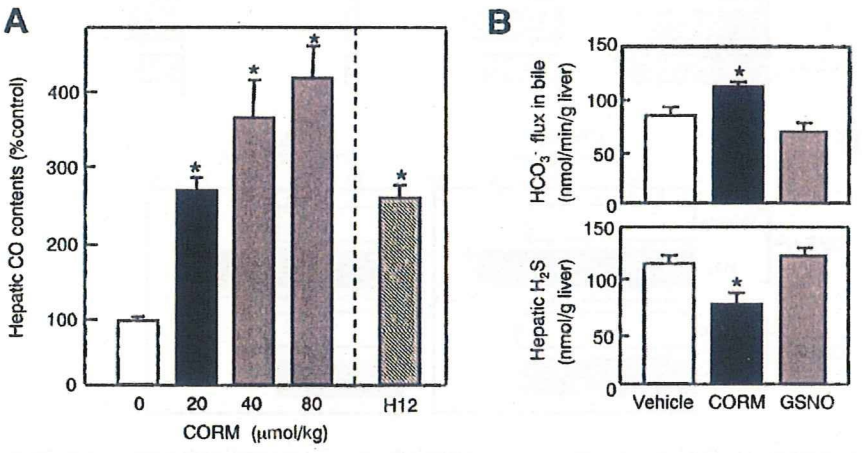

Fig. 4. Effects of the administration of CORM on hepatic CO delivery and biliary function, and their comparison with GSNO, an NO donor. (A) Effects of administration of CORM on hepatic CO contents. H12: the CO contents measured at 12 hours after an intraperitoneal injection of hemin at 40 μmol/kg. Data indicate mean ± SE of five separate experiments for each group. *$P < 0.05$ versus the controls. Note that 20 μmol/kg CORM caused an increase comparable to that induced by H12. (B) Effects of an intraportal administration of CORM on hepatic H_2S contents and biliary HCO_3^- flux. GSNO, S-nitrosyl glutathione, an NO donor. *$P < 0.05$ versus the values in the vehicle-treated controls. Data indicate mean ± SE of seven to eight separate experiments for each group.

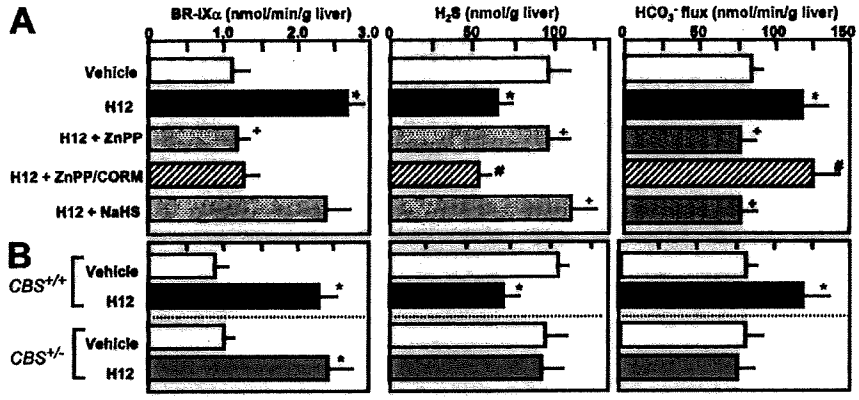

Fig. 5. Effects of HO blockade by zinc protoporphyrin and supplementation of NaHS, an H_2S donor, on biliary flux of BR-IXα, hepatic H_2S contents, and biliary HCO_3^- excretion in the 12-hour hemin-treated liver (H12). (A) Measurements in wild-type male B6 mice. Note that the hemin-induced suppression of H_2S generation and stimulation of biliary HCO_3^- excretion were sensitive to the HO inhibitor and reversed by supplementing CO (CORM). An injection of NaHS, an H_2S donor, restored hepatic H_2S contents and repressed the biliary HCO_3^- excretion in the H12-treated liver, suggesting that the biliary response is H_2S-dependent. (B) Disappearance of H12-induced reduction of H_2S and biliary HCO_3^- excretion in heterozygous CBS-knockout mice ($CBS^{+/-}$). Note that $CBS^{+/-}$ mice neither exhibit a reduction of H_2S nor up-regulate biliary HCO_3^- excretion, although overproducing CO (BR-IXα flux) comparably to the littermates ($CBS^{+/+}$). $*P < 0.05$ versus the vehicle-treated controls. $+P < 0.05$ versus the H12-treated groups. $\#P < 0.05$ versus the H12+ zinc protoporphyrin-treated groups.

has the ability to improve bile acid–dependent bile output of the post–cold ischemic liver grafts through its antioxidative action.[32] However, such an effect of bilirubin appears to be distinct from the stimulatory action of CO on biliary fluid excretion indicated in the current study. CO has been shown to exert diverse actions on biliary function through multiple mechanisms: First, stress-inducible levels of CO have the ability to elongate the intervals of bile canalicular contraction, which helps increase the stroke volume for promoting bile excretion; this process appears to involve mechanisms mediated by modulation of cytochrome P450 epoxygenases and intra-

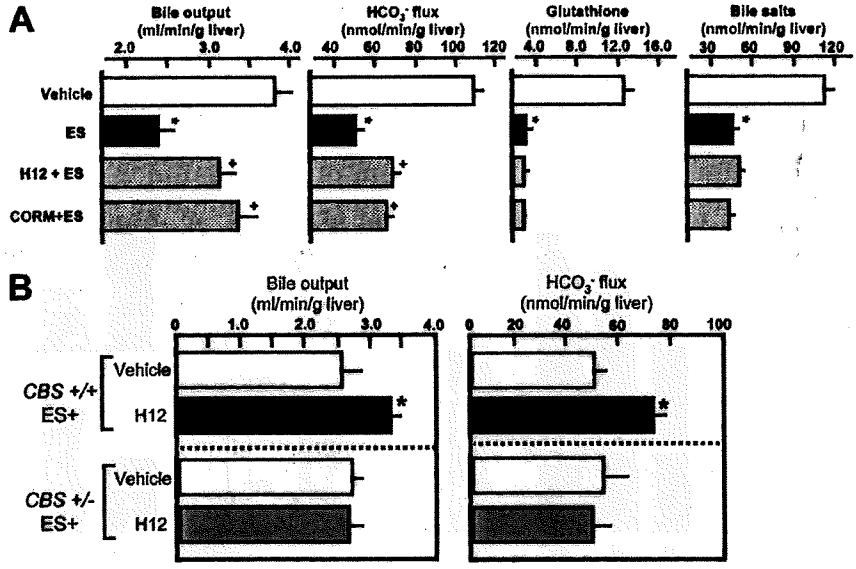

Fig. 6. Effects of H12 treatment or CORM administration on 17α-ethinylestradiol (ES)-induced cholestasis in male B6 mice. (A) Effects of H12 or CORM on ES-induced decreases in the bile output and bile constituents. ES elicited marked cholestasis, which coincided with decreases in HCO_3^-, glutathione, and bile salts in bile. Pretreatment with hemin at 12 hours before the administration of ES (H12 + ES) or the administration of CORM significantly attenuated ES-induced cholestasis through stimulation of HCO_3^- excretion into bile. (B) Effects of H12 treatment on ES-induced impairment of bile output and biliary HCO_3^- flux in $CBS^{+/+}$ and $CBS^{+/-}$ mice. $*P < 0.05$ versus the values in vehicle-treated controls. $+P < 0.05$ versus the values in ES-treated group. Data indicate mean ± SE of eight separate experiments for each group. Note disappearance of the improving effect of H12 treatment in the $CBS^{+/-}$ mice.

cellular Ca^{2+} mobilization.[12] Second, suppression of endogenous CO activates bile acid–dependent bile excretion through accelerated vesicular transport of taurocholate, while inducing no significant elevation of the bile acid–independent fraction.[33] Conversely, CO overproduction by the HO-1 induction or exogenous administration of CO stimulates bile acid–independent choleresis concurrently with increased mrp2-dependent excretion of bilirubin-IXα and glutathione, while suppressing biliary excretion of bile salts, indicating the effects of the gas for stimulating fluid excretion into bile.[34] Of interest is that glibenclamide, an inhibitor of K^+ channel that serves as a putative target for H_2S,[26] acts on Na^+-K^+-$2Cl^-$ cotransporter in bile duct epithelium to stimulate biliary HCO_3^- excretion in normal and cholestatic livers.[35] We showed that inhibition of cystathionine γ-lyase, another H_2S-generating enzyme, stimulates basal and glibenclamide-induced fluid output of bile through stimulating HCO_3^- excretion without altering the baseline vascular resistance of the liver.[14] Recent studies provided evidence that such a glibenclamide-responsive channel is present in rodent cholangiocytes[36] or in duodenum,[37] contributing to stimulation of the HCO_3^- excretion.[36] Based on these observations, it is not unreasonable to speculate that CO stimulates biliary fluid excretion through mechanisms involving H_2S-mediated modulation of glibenclamide-sensitive channels on biliary epithelium. Although further investigation is necessary to determine whether these mechanisms are sensitive to H_2S, the current results shed light on a possibility that the CO-CBS system serves as a putative mechanism for stimulating bile acid–independent fluid excretion, facilitating excretion of HCO_3^- and organic anions such as bilirubin to support heme detoxification. Both glibenclamide and CO help biliary fluid excretion in estrogen-induced hepatocellular cholestasis. Exploration of H_2S-sensitive molecular targets occurring on biliary epithelium deserves further studies for evidence that HO-1–derived CO serves as a therapeutic stratagem for protecting against cholestasis.

CO has been believed to share varied physiological effects on biological systems with NO. However, through extrapolation of studies *in vitro* indicating biochemical actions of CO to trigger structural changes in gas-responsive heme proteins (such as sGC, hemoglobin) distinct from those elicited by NO,[7,19,21,22,38] evidence that CO is a unique gaseous regulator distinct from NO has been emerging. In fact, CO itself modestly activates sGC, by which hepatic sinusoids are constitutively dilated.[2,20,39] By contrast, in vascular smooth muscle cells in which NO is sufficiently supplied from arteriolar endothelium (for example, brain microcirculation), the inducible CO inhibits NO-elicited sGC activation.[40,41] Besides these observations suggesting physiologic actions of CO occurring dependently of local NO levels, the current study provided evidence for a novel mechanism functioning irrespective of the NO effects. Furthermore, our results shed light on a metabolic link between CO and H_2S, suggesting that different gaseous mediators constitute an intriguing link for regulation of organ functions.

Acknowledgment: The authors thank Kayo Maruyama for technical support in measuring tissue H_2S contents.

References

1. Verma A, Hirsch DJ, Glatt CE, Ronnett GV, Snyder SH. Carbon monoxide: a putative neural messenger. Science 1993;259:381-384.
2. Suematsu M, Goda N, Sano T, Kashiwagi S, Egawa T, Shinoda Y, et al. Carbon monoxide: an endogenous modulator of sinusoidal tone in the perfused rat liver. J Clin Invest 1995;96:2431-2437.
3. Ozawa N, Goda N, Makino N, Yamaguchi T, Yoshimura Y, Suematsu M. Leydig cell-derived heme oxygenase-1 regulates apoptosis of premeiotic germ cells in response to stress. J Clin Invest 2002;109:457-467.
4. Song R, Zhou Z, Kim PK, Shapiro RA, Liu F, Ferran C, et al. Carbon monoxide promotes Fas/CD95-induced apoptosis in Jurkat cells. J Biol Chem 2004;279:44327-44334.
5. Mori M, Suematsu M, Kyokane T, Sano T, Suzuki H, Yamaguchi T, et al. Carbon monoxide-mediated alterations in paracellular permeability and vesicular transport in acetaminophen-treated perfused rat liver. HEPATOLOGY 1999;30:160-168.
6. Kyokane T, Norimizu S, Taniai H, Yamaguchi T, Takeoka S, Tsuchida E, et al. Carbon monoxide from heme catabolism protects against hepatobiliary dysfunction in endotoxin-treated rat liver. Gastroenterology 2001;120:1227-1240.
7. Zhao Y, Brandish PE, Ballou DP, Marletta MA. A molecular basis for nitric oxide sensing by soluble guanylate cyclase. Proc Natl Acad Sci U S A 1999;96:14753-14758.
8. Otterbein LE, Bach FH, Alam J, Soares M, Tao Lu H, Wysk M, et al. Carbon monoxide has anti-inflammatory effects involving the mitogen-activated protein kinase pathway. Nat Med 2000;6:422-428.
9. Abraham NG, Quan S, Mieyal PA, Yang L, Burke-Wolin T, Mingone CJ, et al. Modulation of cGMP by human HO-1 retrovirus gene transfer in pulmonary microvessel endothelial cells. Am J Physiol Lung Cell Mol Physiol 2002;283:L1117-L1124.
10. Hill M, Pereira V, Chauveau C, Zagani R, Remy S, Tesson L, et al. Heme oxygenase-1 inhibits rat and human breast cancer cell proliferation: mutual cross inhibition with indoleamine 2,3-dioxygenase. FASEB J 2005;19:1957-1968.
11. Thomas SR, Mohr D, Stocker R. Nitric oxide inhibits indoleamine 2,3-dioxygenase activity in interferon-gamma primed mononuclear phagocytes. J Biol Chem 1994;269:14457-14464.
12. Shinoda Y, Suematsu M, Wakabayashi Y, Suzuki T, Goda N, Saito S, et al. Carbon monoxide as a regulator of bile canalicular contractility in cultured rat hepatocytes. HEPATOLOGY 1998;28:286-295.
13. Wakabayashi Y, Takamiya R, Mizuki A, Kyokane T, Goda N, Yamaguchi T, et al. Carbon monoxide overproduced by heme oxygenase-1 causes a reduction of vascular resistance in perfused rat liver. Am J Physiol 1999;277:G1088-G1096.
14. Fujii K, Sakuragawa T, Kashiba M, Sugiura Y, Kondo M, Maruyama K, et al. Hydrogen sulfide as an endogenous modulator of biliary bicarbonate excretion in the rat liver. Antioxid Redox Signal 2005;7:788-794.
15. Vreman HJ, Wong RJ, Kadotani T, Stevenson DK. Determination of carbon monoxide (CO) in rodent tissue: effect of heme administration and environmental CO exposure. Anal Biochem 2005;341:280-289.

16. Motterlini R, Clark JE, Foresti R, Sarathchandra P, Mann BE, Green CJ. Carbon monoxide-releasing molecules: characterization of biochemical and vascular activities. Circ Res 2002;90:e17-e24.
17. Bossard R, Stieger B, O'Neill B, Fricker G, Meier PJ. Ethinylestradiol treatment induces multiple canalicular membrane transport alterations in rat liver. J Clin Invest 1993;91:2714-2720.
18. Soga T, Baran R, Suematsu M, Ueno Y, Ikeda S, Sakurakawa T, et al. Differential metabolomics reveals ophthalmic acid as an oxidative stress biomarker indicating hepatic glutathione consumption. J Biol Chem 2006;281:16768-16776.
19. Kinoshita A, Tsukada K, Soga T, Hishiki T, Ueno Y, Nakayama Y, et al. Roles of hemoglobin allostery in hypoxia-induced metabolic alterations in erythrocytes: simulation and its verification by metabolome analysis. J Biol Chem 2007;282:10731-10741.
20. Goda N, Suzuki K, Naito M, Takeoka S, Tsuchida E, Ishimura Y, et al. Distribution of heme oxygenase isoforms in rat liver: topographic basis for carbon monoxide-mediated microvascular relaxation. J Clin Invest 1998; 101:604-612.
21. Yonetani T, Tsuneshige A, Zhou Y, Chen X. Electron paramagnetic resonance and oxygen binding studies of alpha-nitrosyl hemoglobin: a novel oxygen carrier having NO-assisted allosteric functions. J Biol Chem 1998; 273:20323-20333.
22. Suganuma K, Tsukada K, Kashiba M, Tsuneshige A, Furukawa T, Kubota T, et al. Erythrocytes with T-state-stabilized hemoglobin as a therapeutic tool for postischemic liver dysfunction. Antioxid Redox Signal 2006;8: 1847-1855.
23. Meier M, Janosik M, Kery V, Kraus JP, Burkhard P. Structure of human cystathionine beta-synthase: a unique pyridoxal 5'-phosphate-dependent heme protein. EMBO J 2001;20:3910-3916.
24. Taoka S, Banerjee R. Characterization of NO binding to human cystathionine beta-synthase: possible implications of the effects of CO and NO binding to the human enzyme. J Inorg Biochem 2001;87:245-251.
25. Prudova A, Bauman Z, Braun A, Vitvitsky V, Lu SC, Banerjee R. S-adenosylmethionine stabilizes cystathionine beta-synthase and modulates redox capacity. Proc Natl Acad Sci USA 2006;103:6489-6494.
26. Zhao W, Zhang J, Lu Y, Wang R. The vasorelaxant effect of H_2S as a novel endogenous gaseous K_{ATP} channel opener. EMBO J 2001;20:6008-6016.
27. Werstuck GH, Lentz SR, Dayal S, Hossain GS, Sood SK, Shi YY, et al. Homocysteine-induced endoplasmic reticulum stress causes dysregulation of the cholesterol and triglyceride biosynthetic pathways. J Clin Invest 2001;107:1263-1273.
28. Maher JM, Dieter MZ, Aleksunes LM, Slitt AL, Guo G, Tanaka Y, et al. Oxidative and electrophilic stress induces multidrug resistance-associated protein transporters via the nuclear factor-E2-related factor-2 transcriptional pathway. HEPATOLOGY 2007;46:1597-1610.
29. Sasaki H, Sato H, Kuriyama-Matsumura K, Sato K, Maebara K, Wang H, et al. Electrophile response element-mediated induction of the cystine/glutamate exchange transporter gene expression. J Biol Chem 2002;277: 44765-44771.
30. Fiorucci S, Antonelli E, Mencarelli A, Orlandi S, Renga B, Rizzo G, et al. The third gas: H_2S regulates perfusion pressure in both the isolated and perfused normal rat liver and in cirrhosis. HEPATOLOGY 2005;42:539-548.
31. Suematsu M, Ishimura Y. The heme oxygenase-carbon monoxide system: a regulator of hepatobiliary function. HEPATOLOGY 2000;31:3-6.
32. Kato Y, Shimazu M, Kondo M, Uchida K, Kumamoto Y, Wakabayashi G, et al. Bilirubin rinse: a simple protectant against the rat liver graft injury mimicking heme oxygenase-1 preconditioning. HEPATOLOGY 2003;38:364-373.
33. Sano T, Shiomi M, Wakabayashi Y, Shinoda Y, Goda N, Yamaguchi T, et al. Endogenous carbon monoxide suppression stimulates bile acid-dependent biliary transport in perfused rat liver. Am J Physiol 1997;272:G1268-G1275.
34. Norimizu S, Kudo A, Kajimura M, Ishikawa K, Taniai H, Yamaguchi T, et al. Carbon monoxide stimulates mrp2-dependent excretion of bilirubin-IXα into bile in the perfused rat liver. Antioxid Redox Signal 2003;5:449-456.
35. Nathanson MH, Burgstahler AD, Mennone A, Dranoff JA, Rios-Velez L. Stimulation of bile duct epithelial secretion by glybenclamide in normal and cholestatic rat liver. J Clin Invest 1998;101:2665-2676.
36. Spirli C, Fiorotto R, Song L, Santos-Sacchi J, Okolicsanyi L, Masier S, et al. Glibenclamide stimulates fluid secretion in rodent cholangiocytes through a cystic fibrosis transmembrane conductance regulator-independent mechanism. Gastroenterology 2005;129:220-233.
37. Sellers ZM, Mann E, Smith A, Ko KH, Giannella R, Cohen MB, et al. Heat-stable enterotoxin of Escherichia coli (STa) can stimulate duodenal HCO_3^- secretion via a novel GC-C- and CFTR-independent pathway. FASEB J 2008;22:1306-1316.
38. Boon EM, Huang SH, Marletta MA. A molecular basis for NO selectivity in soluble guanylate cyclase. Nat Chem Biol 2005;1:53-59.
39. Kajimura M, Shimoyama M, Tsuyama S, Suzuki T, Kozaki S, Takenaka S, et al. Visualization of gaseous monoxide reception by soluble guanylate cyclase in the rat retina. FASEB J 2003;17:506-508.
40. Imai T, Morita T, Shindo T, Nagai R, Yazaki Y, Kurihara H, et al. Vascular smooth muscle cell-directed overexpression of heme oxygenase-1 elevates blood pressure through attenuation of nitric oxide-induced vasodilation in mice. Circ Res 2001;89:55-62.
41. Ishikawa M, Kajimura M, Adachi T, Maruyama K, Makino N, Goda N, et al. Carbon monoxide from heme oxygenase-2 is a tonic regulator against NO-dependent vasodilatation in the adult rat cerebral microcirculation. Circ Res 2005;97:e104-e114.

APPLIED AND ENVIRONMENTAL MICROBIOLOGY, May 2008, p. 2787–2796 Vol. 74, No. 9
0099-2240/08/$08.00+0 doi:10.1128/AEM.01781-07
Copyright © 2008, American Society for Microbiology. All Rights Reserved.

Development of Bottom-Fermenting *Saccharomyces* Strains That Produce High SO_2 Levels, Using Integrated Metabolome and Transcriptome Analysis[▽]

Satoshi Yoshida,[1]* Jun Imoto,[2] Toshiko Minato,[1] Rie Oouchi,[1] Mao Sugihara,[3] Takeo Imai,[3] Tatsuji Ishiguro,[1] Satoru Mizutani,[1] Masaru Tomita,[2] Tomoyoshi Soga,[2] and Hiroyuki Yoshimoto[1]

Central Laboratories for Frontier Technology, KIRIN Holdings Co., Ltd., 1-13-5 Fukuura Kanazawa-ku, Yokohama-shi, Kanagawa 236-0004, Japan[1]; Institute for Advanced Biosciences, Keio University, 246-2 Mizukami Kakuganji, Tsuruoka-shi, Yamagata 997-0052, Japan[2]; and Research Laboratories for Brewing, KIRIN Brewery Co., Ltd., 1-17-1 Namamugi Tsurumi-ku, Yokohama-shi, Kanagawa 230-8628, Japan[3]

Received 1 August 2007/Accepted 24 February 2008

Sulfite plays an important role in beer flavor stability. Although breeding of bottom-fermenting *Saccharomyces* strains that produce high levels of SO_2 is desirable, it is complicated by the fact that undesirable H_2S is produced as an intermediate in the same pathway. Here, we report the development of a high-level SO_2-producing bottom-fermenting yeast strain by integrated metabolome and transcriptome analysis. This analysis revealed that *O*-acetylhomoserine (OAH) is the rate-limiting factor for the production of SO_2 and H_2S. Appropriate genetic modifications were then introduced into a prototype strain to increase metabolic fluxes from aspartate to OAH and from sulfate to SO_2, resulting in high SO_2 and low H_2S production. Spontaneous mutants of an industrial strain that were resistant to both methionine and threonine analogs were then analyzed for similar metabolic fluxes. One promising mutant produced much higher levels of SO_2 than the parent but produced parental levels of H_2S.

The bottom-fermenting yeast *Saccharomyces pastorianus* is used to produce beer and has been proposed to be a natural hybrid between *Saccharomyces cerevisiae* and *Saccharomyces bayanus* (30). Bottom-fermenting yeasts have two types of genes, one set highly homologous (more than 90% identity) to those of *S. cerevisiae* and the other less so but highly homologous to *S. bayanus* (i.e., non-*S. cerevisiae* [Lg type]) (8, 14, 27, 33). One way in which *S. pastorianus* differs from baker's yeast (*S. cerevisiae*) is its tendency to produce higher levels of both sulfite (SO_2) and hydrogen sulfide (H_2S).

It is well known that sulfur compounds in beer make significant contributions to flavor and aroma. SO_2, for example, acts as an antioxidant, which slows the development of oxidation haze and staling of flavors in beer. In contrast, H_2S has an aroma of rotten eggs and is also a precursor of other compounds with undesirable sensory characteristics. SO_2 and H_2S are produced by yeast during reductive sulfate assimilation (Fig. 1). Inorganic sulfate is taken up through a sulfate permease and reduced to SO_2 by enzymes encoded by *MET3*, *MET14*, and *MET16*. SO_2 is then reduced to H_2S by SO_2 reductase encoded by *MET5* and *MET10* (29). The next intermediate, homocysteine, which is synthesized from H_2S and *O*-acetylhomoserine (OAH) by OAH sulfhydrylase encoded by *MET17*, leads to the formation of cysteine, methionine, and *S*-adenosylmethionine (SAM). SAM transcriptionally represses all of the genes involved in sulfate assimilation. Park and Bakalinsky previously reported that *SSU1* encodes an SO_2 efflux pump that exports intracellular SO_2 through the plasma membrane (18).

In the postgenomic era, systematic and high-throughput analyses of mRNA and proteins have become central to recent functional genomics initiatives. Metabolomics entails the analysis of all cellular metabolites and has become a powerful new tool for gaining insight into functional biology. Measurement of numerous metabolites within a cell and tracking concentration changes as a function of growth or environmental conditions not only provides direct information on metabolic phenotypes but also complements gene expression and proteomic studies. Current large-scale methods for the analysis of metabolites are based on gas chromatography (GC)-mass spectrometry (MS) (7), liquid chromatography-MS (31), nuclear magnetic resonance (20), and Fourier transform ion cyclotron resonance-MS (1). Recently, capillary electrophoresis-electrospray ionization (CE-ESI)-MS has emerged as a powerful analytical tool, and a number of CE-ESI-MS methods have been developed for the analysis of charged species such as carboxylic acids, phenolic compounds, amino acids, metal species, tetramines, and herbicides (25). While metabolite-profiling analysis of the glutathione synthesis pathway in baker's yeast was recently reported (15), to our knowledge, the metabolomic analysis of bottom-fermenting yeast has not yet been reported.

The physiology of sulfur metabolism in *Saccharomyces* yeasts, particularly in regard to SO_2 and H_2S production, has received significant attention (11, 17, 28). Although the biosynthesis of these two compounds is interconnected, it would be desirable to increase SO_2 and to decrease H_2S in beer. Yeast strains that produce lowered levels of H_2S have been

* Corresponding author. Mailing address: Central Laboratories for Frontier Technology, KIRIN Holdings Co., Ltd., 1-13-5 Fukuura Kanazawa-ku, Yokohama-shi, Kanagawa 236-0004, Japan. Phone: 81-45-330-9003. Fax: 81-45-788-4042. E-mail: satoshiy@kirin.co.jp.

▽ Published ahead of print on 29 February 2008.

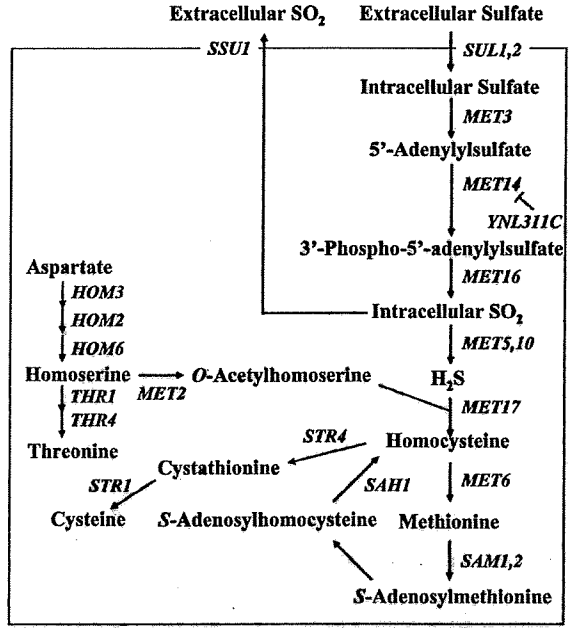

FIG. 1. Schematic of the reductive sulfate assimilation pathway in yeast. *YNL311C* encodes an F-box protein (13). Ynl311c negatively regulates Met14 and degrades it via a ubiquitin-related pathway.

constructed or isolated by gene disruption, conventional mutagenesis, and cell fusion techniques. However, those treatments have also resulted in undesirable phenotypes (11). Mutants that produce higher levels of SO_2 have been obtained by the overexpression of *SSU1* and/or *MET14* (4) and by the disruption of *MET10* (11). However, bottom-fermenting yeast strains in which *MET10* was disrupted were also found to have acquired undesirable phenotypes (11), possibly due to a reduction in intracellular methionine or slow growth. Furthermore, because these yeasts were obtained by the use of recombinant DNA technology, they cannot be used commercially.

In this paper, we report integrated metabolome and transcriptome analysis of reductive sulfate assimilation in baker's and bottom-fermenting yeasts. Based on these data, we proposed that OAH is one of the rate-limiting factors for SO_2 and H_2S production, and we constructed high-level SO_2-producing mutants without increasing H_2S levels by simultaneously increasing the flux from aspartate to OAH and increasing the flux from sulfate to SO_2. One candidate mutant that produced much higher levels of SO_2 than the parent, parental levels of H_2S, and no undesirable changes in fermentation properties was isolated.

MATERIALS AND METHODS

Strains and media. Bottom-fermenting yeast *S. pastorianus* strains used in this study were KBY011 (our laboratory stock), YMO106 (mutant selected from KBY011), and B43 (meiotic segregant of KBY011). Baker's yeast *S. cerevisiae* strains used were S288C (*MAT*α) and SYT001 (*MAT*a; derived from DBY7286). Strains were grown in YPD (1% yeast extract, 2% peptone, and 2% glucose), YPD10 (1% yeast extract, 2% peptone, and 10% glucose), SD10 (0.4% yeast nitrogen base without amino acids and ammonium sulfate, 0.2% ammonium sulfate, and 10% glucose), SD10(2) (0.2% yeast nitrogen base without amino acids and ammonium sulfate, 0.1% ammonium sulfate, and 10% glucose), or Brewer's wort. Strains and media used in each experiment are shown in Table 1. YPDL plates (0.5% yeast extract, 0.3% peptone, 4% glucose, 0.02% ammonium sulfate, 0.1% lead nitrate, and 2% agar) were used to test for H_2S production (9). SDLE plates (0.17% yeast nitrogen base without amino acids and ammonium sulfate, 0.5% ammonium sulfate, 2% glucose, 0.1% lead nitrate, 10 mg/ml DL-ethionine, and 2% agar) and SDH medium (0.17% yeast nitrogen base without amino acids and ammonium sulfate, 0.5% ammonium sulfate, 2% glucose, and 100 mg/ml of DL-hydroxynorvaline) were used to isolate mutants. Geneticin (G418) at 200 μg/ml, blasticidin S at 50 μg/ml, or aureobasidin A at 1 μg/ml was added to YPD plates to select and screen transformants. Transformation of yeast strains was carried out by use of a modified gene pulser procedure (16).

Isolation of meiotic segregant from bottom-fermenting yeast. Meiotic segregants were obtained from KBY011 as described previously by Bilinski et al. (2). With respect to SO_2 and H_2S production, the meiotic segregant B43 is similar to KBY011.

Isolation of mutants resistant to amino acid analogs. Wild-type cells were incubated in 5 ml of YPD at 20°C for 3 days. After centrifugation, cells were resuspended in 5 ml of distilled water. One hundred fifty microliters of cells was spread onto SDLE plates and incubated at 20°C for 10 days. Ethionine-resistant mutants were incubated in 5 ml of YPD at 20°C for 3 days. After centrifugation, the cells were resuspended in 10 ml of distilled water. One hundred microliters of cells was added to SDH and incubated at 20°C for 5 days. One hundred microliters of culture was spread onto YPDL plates, which were then incubated at 20°C for 7 days.

Construction of overexpression plasmids. To construct pYES-G418GP, a 1.5-kb SalI fragment containing a *GPD* promoter and *PGK1* terminator cassette derived from pSY114 (32) was inserted at the SalI site of pYES-G418 (34). To construct plasmids overexpressing *S. cerevisiae MET14* (Sc*MET14*), Sc*HOM3*, Lg*HOM3*, Lg*MET17*, and Lg*THR1*, these genes were cloned by PCR using KBY011 genomic DNA and inserted at the BamHI site of pYES-G418GP. To construct the integration vector pAUR-HOM3, Sc*HOM3* was inserted into the BamHI site of pSY114, and a 3-kb *GPD* promoter-Sc*HOM3-PGK* terminator cassette was inserted at the SalI site of pAUR101 (Takara Shuzo) carrying an aureobasidin A resistance marker. Integration of the Sc*HOM3* gene was confirmed by Southern hybridization analysis.

Construction of disruption plasmids. To disrupt both Lg and *S. cerevisiae* types of *YNL311C* and *HOM3* genes in B43, the Lg*YNL311C* gene was cloned from a KBY011 cosmid library based on homology with the corresponding *S. cerevisiae* genes. To construct a vector harboring a blasticidin S resistance cassette, a 0.5-kb HindIII fragment carrying blasticidin S resistance was inserted at the HindIII site of pSY114 carrying a *GPD* promoter and a *PGK* terminator. This blasticidin S resistance expression cassette was then integrated into the open reading frames of the Lg*YNL311C* and Lg*HOM3* genes, respectively. The corresponding *S. cerevisiae*-type genes were disrupted by DNA fragments amplified using genomic DNA derived from the yeast knockout strains (Open Biosystems). Disruption of both types of genes was confirmed by PCR.

Growth conditions for comprehensive analyses. KBY011 and S288C were precultured with shaking at 20°C for 3 days in 500 ml of YPD10. Cells were harvested and diluted to a density of 0.5% (wt/vol) in 2 liters of fresh SD10 and grown with gentle stirring at 20°C for 3 days under anaerobic conditions produced by initial headspace exclusion and N_2 flushing. Cells were then harvested, diluted to a density of 0.5% (wt/vol) in 2 liters of the fresh SD10, and grown at 20°C under anaerobic conditions with gentle stirring (experiment 1). To test the effect of the addition of threonine, SYT001 cells were harvested and diluted to a density of 0.5% (wt/vol) in 2 liters of fresh SD10(2) with or without 1 g/liter of threonine and grown at 20°C under anaerobic conditions with gentle stirring. Cells were then collected at different time points (0, 6, 24, and 48 h) and harvested for metabolome analysis (experiment 2).

Growth conditions for small-scale fermentation. B43, KBY011, and YMO106 were precultured with shaking at 20°C for 3 days in 500 ml of YPD10 (200 mg/liter of G418 was added in experiment 3). Cells were harvested, diluted to a

TABLE 1. Strains and media used in this study

Expt	Strain(s)	Medium
1	S288C and KBY011	SD10
2	SYT001	SD10(2) with or without threonine
3	B43 and derivatives	YPD10 + G418
4	B43 and derivatives	YPD10
5	KBY011 and YMO106	Wort

density of 0.5% (wt/vol) in 200 ml of fresh YPD10 (experiments 3 and 4) or 500 ml of wort (experiment 5), and grown at 20°C for 4 days under anaerobic conditions produced by initial headspace exclusion and N_2 flushing. Cells were then harvested, diluted to a density of 0.5% (wt/vol) in 200 ml of fresh YPD10 or 500 ml of wort, and grown with gentle stirring at 20°C under anaerobic conditions.

DNA microarray analysis. DNA microarray experiments were carried out using bottom-fermenting yeast oligoarrays (Agilent DNA microarray system). Oligonucleotide probes (60 bp) were spotted onto the array, which carries 3,181 probes derived from Lg-type genes and 6,637 probes derived from *S. cerevisiae* genes. Total RNA was extracted using glass beads (21) and purified using an RNeasy column (Qiagen), and 0.2 μg of RNA was labeled using the Agilent linear amplification/labeling kit (Agilent Technologies) according to the manufacturer's instructions. Hybridization of labeled cRNA to the arrays was performed using the manufacturer's hybridization protocol. Microarrays were washed, dried, and scanned on a dual-laser DNA microarray scanner (model G2565BA; Agilent Technologies). Feature Extraction and Image Analysis software programs were used. Normalization was carried out by the Lowess method. For each experiment, the data presented are hybridization means for two arrays in two-dye swap experiments (i.e., Cy3 and Cy5 dye-swapping experiments).

Extraction of intracellular metabolite. Metabolites were extracted using a modification of a previously described procedure (25). Cells were harvested from a culture medium (optical density at 600 nm of 30) by filtration through a 0.45-μm-pore-size filter. Methionine sulfone and 2-morpholinoethanesulfonic acid (MES) were used as internal cationic and anionic standards, respectively. Lyophilized samples were dissolved in 50 μl of Milli-Q water before CE-ESI-MS analysis.

CE-ESI-MS conditions for metabolite analysis. All CE-ESI-MS experiments were performed using an Agilent capillary electrophoresis system equipped with an air pressure pump, an Agilent 1100 series MSD mass spectrometer and an isocratic high-performance liquid chromatography (HPLC) pump, a G1603A Agilent CE-MS adapter kit, and a G1607A Agilent CE-ESI-MS sprayer kit (Agilent Technologies) as described previously (23, 24).

Other analyses. The supernatants from filtered samples were assayed for free SO_2 and organic acids by HPLC. H_2S was detected quantitatively using a headspace GC-sulfur chemiluminescence detector system. Higher alcohols, esters, acetaldehyde, and diacetyl were measured by GC.

Statistical analysis. Each metabolomic experiment (experiments 1 and 2) was done in triplicate in independent experiments, and data were analyzed by using mean values from triplicate samples, except for SO_2 and H_2S. The data below the detection limit were not included for statistical analysis. In experiments involving overproduction of Met14 and Hom3 in B43, significant differences in SO_2 and H_2S production levels between the two strains were compared using Student's *t* test (ystat2006.xls; S. Yamazaki, Igaku Tosho Press, Inc., Japan).

Microarray data accession number. The microarray data are registered in the ArrayExpress (EBI) database under accession number E-MEXP-1086.

RESULTS

Metabolite and gene expression profiling analyses of sulfur metabolism in bottom-fermenting and baker's yeasts. For unknown reasons, bottom-fermenting yeast produces high levels of SO_2 and H_2S under anaerobic conditions, while baker's yeast does not (26). To determine the basis for this difference, we carried out transcriptome and metabolome analyses. SD10 medium lacking amino acids was used to minimize complications resulting from amino acid uptake. Most intracellular metabolites related to sulfate assimilation were measured by CE-ESI-MS, while SO_2 was analyzed by HPLC, and H_2S was analyzed by GC. Figure 2 shows levels of sulfur metabolites in cell extracts and SO_2 and H_2S in media. Because a commercial 3′-phospho-5′-adenylylsulfate standard was not available, 3′-phospho-5′-adenylylsulfate was quantified relative to the internal standard MES. As reported above, the production of extracellular SO_2 and H_2S by bottom-fermenting strain KBY011 was much greater than that by baker's yeast *S. cerevisiae* S288C. In contrast, levels of intracellular OAH and homoserine were much lower in KBY011 than in S288C. Figure 3 shows the expression profiles of genes involved in sulfur metabolism in S288C and KBY011. We constructed the bottom-fermenting yeast microarray based on the expressed sequence tag data for KBY011 (33), because the whole-genome sequence of bottom-fermenting yeast was not available at the time of this writing. Graphs for which a KBY011 data set are missing indicate that the respective probes were unavailable in the expressed sequence tag data. The expression patterns of the *MET2*, *MET14*, and *MET16* genes were found to differ between S288C and KBY011. Furthermore, the expression levels of both the Lg- and *S. cerevisiae*-type *HOM3* genes were much lower in KBY011 than in S288C in the early stage of fermentation. Based on the metabolome and transcriptome data, we suggest that KBY011 has a lower level of OAH than S288C, probably due to the low level of expression of *HOM3* or related enzyme activities. We presume that KBY011 may produce higher levels of SO_2 and H_2S than S288C due to limiting amounts of OAH, which reacts with H_2S to form homocysteine.

OAH is rate limiting for H_2S production. To test the hypothesis that OAH is a rate-limiting factor for SO_2 and H_2S production, we performed the experiments described below. It was reported previously that in yeast, threonine inhibits aspartate kinase encoded by *HOM3* through feedback inhibition (6) and that the addition of threonine increases SO_2 production (10), suggesting that the addition of threonine would shift the pattern of sulfate assimilation in baker's yeast to that observed in bottom-fermenting yeast. Therefore, metabolome analysis of baker's yeast strain SYT001 grown in SD10(2) was performed with and without added threonine. As expected, the addition of threonine caused elevated levels of SO_2 and H_2S production, especially 24 h after the addition (Fig. 4). The metabolome data show that homoserine and OAH levels were lower in the presence of added threonine than in the absence of threonine (Fig. 4). These results are consistent with threonine feedback-inhibiting aspartate kinase leading to a decrease in OAH production and a resulting increase in SO_2 and H_2S levels.

Moreover, the effect of the addition of OAH on H_2S production was tested on YPDL plates using KBY011. Figure 5 shows that threonine increased H_2S production, while homoserine and OAH decreased H_2S production at a final concentration of 1 mM. These results strongly suggest that OAH is a rate-limiting factor for H_2S production.

Effect of overexpression and disruption of genes involved in sulfate assimilation. As noted above, OAH appears to be the rate-limiting factor for SO_2 and H_2S production. SO_2 and H_2S production are linked (5), as SO_2 is the immediate biochemical precursor of H_2S in the reductive sulfate assimilation pathway (Fig. 1), indicating that flux from sulfate to SO_2 is important for both SO_2 and H_2S production. Therefore, the effects of genetically altering the flux from aspartate to OAH and the flux from sulfate to SO_2 on SO_2 and H_2S production were investigated using relevant overexpressed and disrupted genes. As bottom-fermenting yeast is proposed to be a tetraploid, meiotic segregants expected to each have a set of *S. cerevisiae*-type and Lg-type genes from KBY011 were isolated to make the experiment more tractable. One of them, B43, exhibited sulfur metabolism and a fermentation profile similar to those of parent strain KBY011 (data not shown).

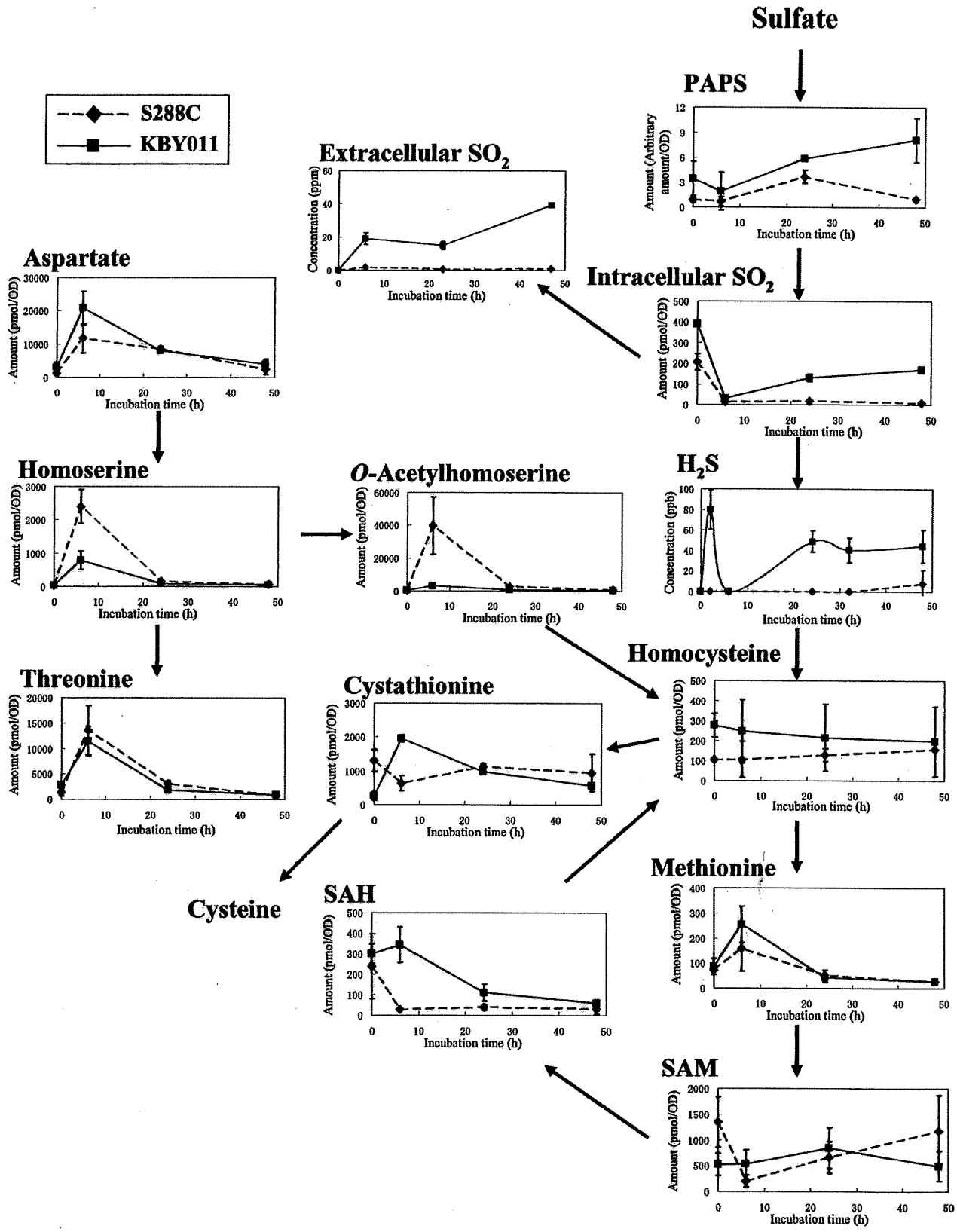

FIG. 2. Changes in metabolite pools related to reductive sulfate assimilation in bottom-fermenting and baker's yeasts. Extracellular SO_2 and H_2S levels are concentrations in the spent media. Concentrations of the other metabolites (pmol) are expressed per unit yeast biomass (an amount of cells equivalent to an optical density [OD] at 600 nm of 1). The data are means of three independent experiments, with the error bars indicating standard deviations. Diamonds and squares indicate baker's yeast (S288C) and bottom-fermenting yeast (KBY011), respectively (experiment 1). SAH, *S*-adenosylhomocysteine; PAPS, 3′-phospho-5′-adenylylsulfate.

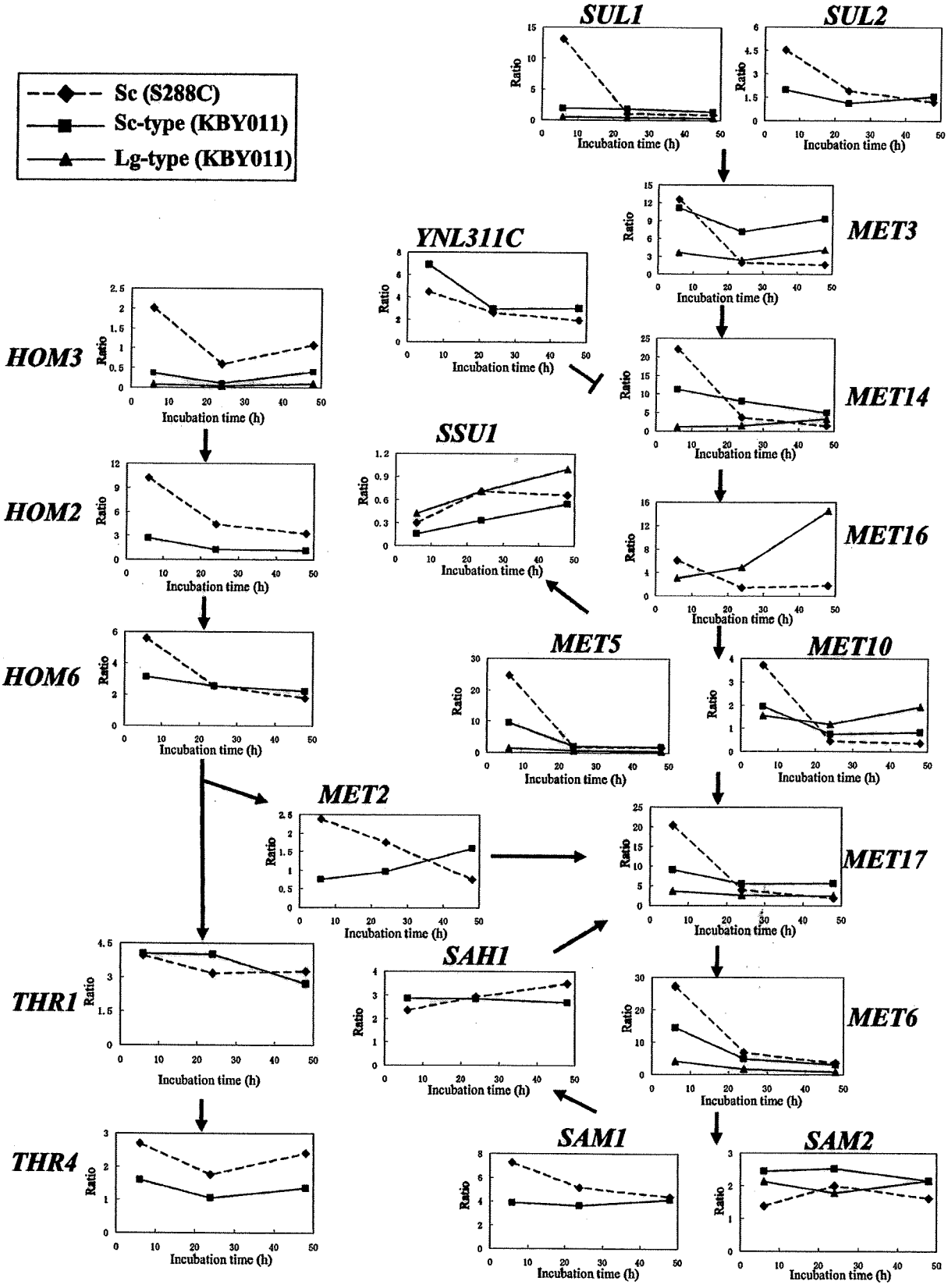

FIG. 3. Changes in expression levels of genes involved in reductive sulfate assimilation in bottom-fermenting and baker's yeasts. Diamonds, squares, and triangles indicate baker's yeast, bottom-fermenting yeast *S. cerevisiae* (Sc)-type, and bottom-fermenting yeast Lg-type genes, respectively (experiment 1). The *y* axis is the expression ratio relative to the zero time point. These microarray data are means of analyses taken from two independent fermentation experiments with very similar results (experiment 1).

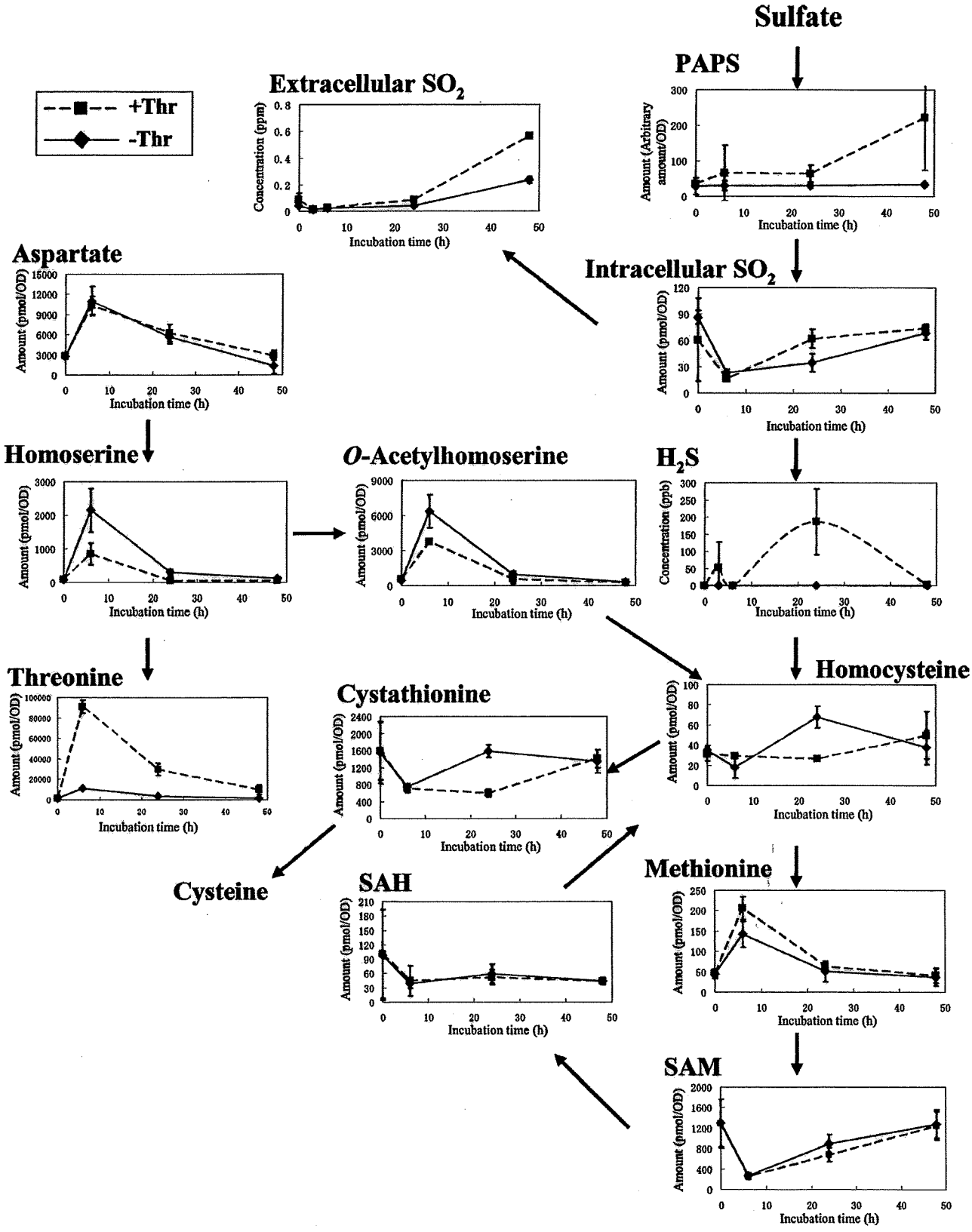

FIG. 4. Changes in metabolite pools related to reductive sulfate assimilation in baker's yeast with or without threonine. Concentrations of metabolites are indicated as described in the Fig. 2 legend. The data represent mean values from three independent experiments, with error bars showing standard deviations. Squares and diamonds indicate baker's yeast with and without the addition of threonine, respectively (experiment 2). SAH, *S*-adenosylhomocysteine; PAPS, 3′-phospho-5′-adenylylsulfate; OD, optical density.

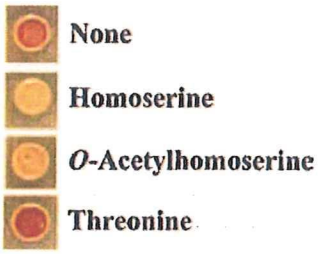

FIG. 5. Effect of OAH on H_2S production in bottom-fermenting yeast. All compounds shown were added to YPDL plates at a final concentration of 1 mM. Cells of bottom-fermenting yeast strain KBY011 were incubated at 25°C on YPDL plates for 4 days.

Initially, in order to regulate the flux from aspartate to OAH, a B43 strain overexpressing Lg*HOM3*, Lg*MET17*, or Lg*THR1* was constructed. The levels of SO_2 and H_2S of the Lg*HOM3*-overexpressing B43 strain were found to be 1.1- and 3.5-fold lower than those of the control, respectively (Table 2). A *hom3* disruptant was also constructed and evaluated. SO_2 and H_2S levels in the *hom3* disruptant were 2.6- and 2.8-fold higher than those of the parent, respectively (Table 3). These results indicate that the flux from aspartate to OAH has more significant effects on H_2S production than on SO_2 production.

To alter the flux from sulfate to SO_2, a Met14-overproducing strain was constructed by disrupting *YNL311C*. Ynl311c has an F-box motif, interacts with Met14 (13), and is involved in its proteolysis via the ubiquitin pathway (S. Yoshida et al., unpublished results). The levels of SO_2 and H_2S in the *ynl311c* disruptant were found to be 2.5- and 1.6-fold higher, respectively, than those in the controls (Table 3). This indicates that the flux from sulfate to SO_2 has a greater effect on SO_2 production than on H_2S production.

Based on these results, strains producing high SO_2 and low H_2S levels were sought by simultaneously increasing the flux from aspartate to OAH and increasing the flux from sulfate to SO_2.

Breeding of bottom-fermenting yeast by genetic modification and spontaneous mutants resistant to both methionine and threonine analogs. Strain B43, which overproduced both Hom3 and Met14, produced almost same amount of H_2S as the parent strain on YPDL plates (data not shown). The levels of SO_2 and H_2S after the overproduction of Met14 and Hom3 were 2.68 ± 0.22 ppm and 165.4 ± 11.8 ppb, respectively, for the parent strain and 3.86 ± 0.50 ppm ($P < 0.05$) and 131.8 ± 13.3 ppb ($P < 0.05$), respectively, for the Δ*yn1311c* Sc*HOM3* strain, as measured after 24 h (means and standard deviations from three independent experiments [experiment 3] are shown). Similarly, with respect to the simultaneous overexpression of both Sc*MET14* and Sc*HOM3*, the levels of SO_2 and H_2S of the control strain were 1.57 ± 0.56 ppm and 113.1 ± 19.2 ppb, respectively, and those of the strain overexpressing both Sc*MET14* and Sc*HOM3* were 2.55 ± 0.65 ppm ($P < 0.05$) and 88.4 ± 17.4 ppb ($P < 0.05$), respectively, as measured after 23 h (values are means and standard deviations from five independent experiments [experiment 3]). Significant differences between the parent and genetically modified strains were determined by a Student's *t* test. These results indicate that high SO_2 and low H_2S production can be achieved by simultaneously increasing the flux from aspartate to OAH and increasing the flux from sulfate to SO_2.

TABLE 2. Effect of gene overexpression on SO_2 and H_2S production in strain B43[a]

Gene	SO_2 level (ppm)	H_2S level (ppb)
Vector	2.51	118.3
Lg*HOM3*	2.27	33.5
Lg*MET17*	2.24	0
Lg*THR1*	2.58	143.5

[a] SO_2 and H_2S levels were measured after 23 h. The data represent means for two independent experiments (experiment 3).

TABLE 3. Effect of gene disruption on SO_2 and H_2S production in strain B43[a]

Genotype	SO_2 level (ppm)	H_2S level (ppb)
Parent	1.55	102
Δ*hom3*	3.97	290
Δ*ynl311c*	3.89	166

[a] SO_2 and H_2S levels were measured after 24 h (experiment 4).

In order to isolate a spontaneous mutant exhibiting similar metabolic fluxes for commercial use, strains resistant to both methionine and threonine analogs were selected. Initially, we isolated ethionine-resistant mutants from KBY011, whose flux from sulfate to H_2S would be expected to increase. From among 1.4×10^8 cells, 14 ethionine-resistant candidates that formed black colonies on YPDL plates were isolated (Fig. 6A). SO_2 and H_2S productivities were analyzed in three of them. One, YMO2, produced 2.2-fold more SO_2 and 2.4-fold more H_2S than did the parent strain in YPD10 medium. Hydroxynorvaline-resistant mutants of YMO2 were then selected in order to increase the flux from aspartate to OAH. From among 10^8 cells, 10 candidates that formed thin brown colonies were isolated (Fig. 6A). One candidate, YMO106, produced 2.7-fold more SO_2 than did parent strain KBY011 but produced the same amount of H_2S (1.04-fold more) in wort after 24 h of incubation (Fig. 6B). No differences in H_2S accumulation were observed between KBY011 and YMO106 using YPDL plates (Fig. 6A). These results suggest that mutants that produce much higher SO_2 levels but without a significant increase in H_2S levels can be isolated by simultaneously increasing the flux from aspartate to OAH and increasing the flux from sulfate to SO_2. An independently isolated ethionine- and hydroxynorvaline-resistant mutant from a different industrial strain was also found to produce a high level of SO_2 and a low level of H_2S (data not shown). This mutant exhibited almost the same SO_2 and H_2S productivities as the *HOM3*- and *MET14*-overexpressing strain, demonstrating that mutants that produce higher SO_2 and lower H_2S levels can be isolated by the selection of mutants that are resistant to the two-amino-acid analogs.

Lager fermentations using strains KBY011 and YMO106 in 200-liter batches of wort were performed. Chemical analysis of the resultant beers is summarized in Table 4. With respect to SO_2, the beer produced by YMO106 (YMO106 beer) contained much higher levels of SO_2 than that produced by KBY011 (KBY011 beer) at all sampling times. At the end of

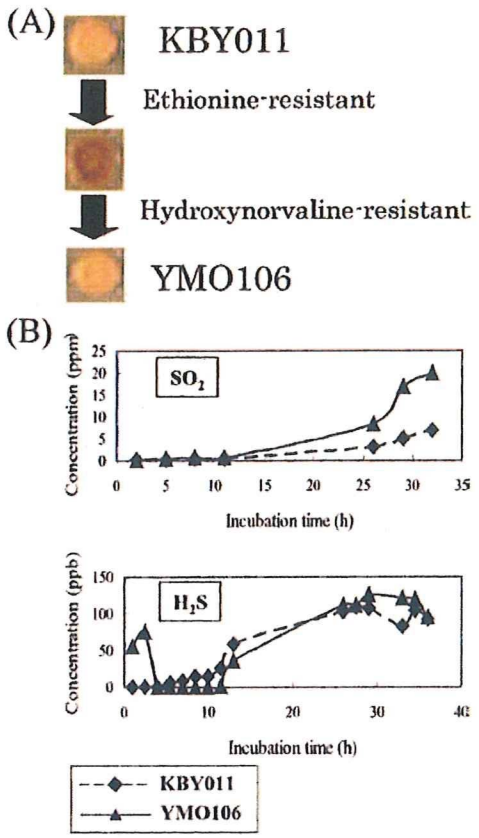

FIG. 6. SO_2 and H_2S production in the spontaneous mutant. (A) Strategy for isolating mutant strain YMO106 from parental strain KBY011. Yeast cells were incubated at 20°C on YPDL plates for 5 days. (B) Extracellular SO_2 and H_2S concentrations in media are shown. Diamonds and triangles indicate parental strain KBY011 and mutant strain YMO106, respectively (experiment 5).

the main fermentation, the YMO106 beer contained less H_2S than did the KBY011 beer, while the opposite was true after a period of maturation. It is more important to decrease H_2S during the main fermentation than during beer maturation, because undesirable compounds derived from H_2S are produced during the main fermentation. The increase in H_2S in the YMO106 beer would be expected to disappear upon longer maturation. The YMO beer contained about the same amount of organic acids and volatile compounds as did the KBY011 beer (diacetyl, acetaldehyde, esters, and fusel alcohols), suggesting that the introduced mutations did not cause undesirable changes in the concentrations of compounds having a major sensory impact in beer (Table 4).

DISCUSSION

Metabolomics, the global analysis of cellular metabolites, is becoming a powerful new tool for gaining insight into biological functions. Analysis of a number of metabolites and tracking concentration changes under various physiological and genetic conditions should provide direct information on metabolic phenotypes complementary to gene expression. Metabolome and transcriptome approaches in this work revealed three main insights. First, OAH is the rate-limiting factor for the production of H_2S. Second, the flux from aspartate to OAH has a greater impact on H_2S production than on SO_2 production, while flux from sulfate to SO_2 has a greater impact on SO_2 production than on H_2S production. Third, the simultaneous increase in the flux from aspartate to OAH and the flux from sulfate to SO_2 resulted in high levels of SO_2 production with no increase in H_2S formation relative to that of the parent.

In order to increase SO_2 and to lower H_2S production, we compared the formations of these metabolites in bottom-fermenting and baker's yeasts. Metabolome data indicated that the bottom-fermenting species produced less OAH, a homocysteine precursor, than did *S. cerevisiae*. One reason for this reduced amount of OAH is possibly due to lower expression levels of *HOM3* in bottom-fermenting yeast, which causes higher SO_2 and lower H_2S productivity, suggesting that OAH is the rate-limiting factor in SO_2 and H_2S production.

Alternative approaches to developing yeast strains that produce higher SO_2 and lower H_2S levels have been proposed. One is the disruption of genes encoding SO_2 reductase subunits or other proteins required for SO_2 reductase function, including *MET5*, *MET10*, *MET1*, and *MET8*. Hansen and Kielland-Brandt reported previously that a *MET10* disruption resulted in high levels of SO_2 production (11). Considering the function of *MET10*, one would have expected lower H_2S levels as well. The overexpression of *SSU1*, encoding a plasma membrane SO_2 efflux pump, has also been proposed to be a means of reducing H_2S levels. The use of a sulfite reductase mutant or a mutant that exports a significant amount of SO_2 in raw

TABLE 4. Levels of SO_2, H_2S, and selected aroma compounds in beer after the main fermentation and in bottled beer after maturation produced by strain KBY011 (parent) and derivative strain YMO106[a]

Compound	Concn														
	SO_2 (fermentation tank) (ppm)	SO_2 (bottled beer) (ppm)	H_2S (fermentation tank) (ppb)	H_2S (bottled beer) (ppb)	Total diacetyl (ppm)	Acetaldehyde (ppm)	Ethyl acetate (ppm)	Amyl alcohol (ppm)	Isoamyl acetate (ppm)	Sulfate (ppm)	Maleic acid (ppm)	Citric acid (ppm)	Succinic acid (ppm)	Lactic acid (ppm)	Acetic acid (ppm)
KBY-1	1.5	1.3	49.0	2.6		7.0	23.8	70.4	2.0	89	96	204	119	97	89
YMO-1	2.2	3.7	30.3	2.0		4.1	18.3	97.4	1.8	100	109	199	116	106	57
KBY-2	2.5	1.6	27.1	2.9	0.04	4.0	21.3	85.0	1.8	110	104	190	85	92	112
YMO-2	7.1	4.2	25.7	3.3	0.04	5.0	23.9	78.2	2.2	99	92	207	96	107	133

[a] KBY-1 and YMO-1 indicate beer produced in the first fermentation by KBY011 and YMO106, respectively. KBY-2 and YMO-2 indicate beer produced in the second fermentation by KBY011 and YMO106, respectively.

materials such as wort that has a limited amino acid content is likely to lead to limited growth due to the depletion of methionine and cysteine. In contrast, in the *HOM3*- and *MET14*-overexpressing strain, intracellular methionine or cysteine was sufficient, as evidenced by the ability of this strain to grow in unsupplemented minimal SD medium. It is possible that the combined overexpression of *SSU1* and *MET14* would work as well as overexpression of *HOM3* and *MET14*. Nonetheless, all the strains described above have been genetically manipulated and therefore are inappropriate for commercial use.

With commercial use in mind, we selected spontaneous mutants that were resistant to both ethionine (methionine analog) and hydroxynorvaline (threonine analog) to obtain a high-level SO_2-producing strain that did not produce increased levels of H_2S. Strain YMO106, which produced higher SO_2 levels but parental levels of H_2S, was selected in this screen. The bottom-fermenting yeast strain in which all *MET10* genes were disrupted produced 13-fold more SO_2 but 5-fold more acetaldehyde, 3-fold more 1-propanol, and 1.7-fold more dimethyl sulfide (DMS) than the parental strain (11). As shown in Table 4, strain YOM106 obtained in this study produced 2.8- and 2.6-fold more SO_2 (fermentation tank and bottled beer produced in the second fermentation, respectively), 1.3-fold more acetaldehyde, and 0.9- and 1.1-fold more H_2S than the parental strain (fermentation tank and bottled beer produced in the second fermentation, respectively). Beer produced by YMO106 was very similar to that produced by the parental strain except for the higher level of SO_2. These results indicate that selection for resistance to amino acid analogs, based on the integration of the metabolome and transcriptome data, was a successful approach for obtaining a high-level SO_2-producing strain. To our knowledge, this is the first report to integrate metabolome and transcriptome data for the development of improved industrial yeast strains.

It is possible that the mutation responsible for ethionine resistance in YMO106 is in *SAM1* or *SAM2*, both of which are involved in the transcriptional regulation of methionine biosynthesis (3, 22), in the methionine permease *MUP1* (12), or in *STR4*, which encodes cystathionine β-synthase (Fig. 1). Previous screening of the yeast gene knockout collection for H_2S-overproducing mutants led to the identification of *mup1* and *str4* deletion mutants (Yoshida et al., unpublished). Mutations in *SAM1* or *SAM2* would also be expected to result in a loss of function because SAM represses the transcription of the methionine biosynthetic genes including *MET3* and *MET14*. However, the *sam1* and *sam2* mutants were not found to overproduce H_2S, possibly because wild-type *SAM1* and *SAM2* complemented *sam2* and *sam1*, respectively, in the single mutants. Nonetheless, it is possible that *SAM1* and *SAM2* might be repressed simultaneously in YMO106. On the other hand, a mutation in *HOM3* might be responsible for hydroxynorvaline resistance, because *HOM3-R2* dominant mutants have been reported to exhibit hydroxynorvaline resistance in *S. cerevisiae* (19). However, as the hydroxynorvaline resistance of YMO106 is weak, it is possible that the mutation is not in *HOM3*. It is possible that the mutation responsible for hydroxynorvaline resistance is in genes involved in threonine uptake or in other genes including *HOM2*, *HOM6*, *MET2*, *MET17*, *THR1*, and *THR4*.

DMS, dimethyl disulfide, methional, and methionol were measured in bottled beers. Relative to KBY011, YMO106 was found to produce 1.6-fold more DMS, 0.6-fold less dimethyl disulfide, 0.6-fold less methional, and 1.5-fold more methionol, indicating minor consequences of the introduced mutation on the methionol synthesis and methionine degradation pathway. Significantly, these values are below taste threshold levels.

Finally, we report herein a method to identify rate-limiting factors in a metabolic pathway by the integration of transcriptome and metabolome data, followed by genetic and nongenetic metabolic engineering to increase desirable end products in yeast. This method should have general application to the problem of increasing the production of useful metabolites while minimizing the simultaneous production of undesirable but related compounds derived from a linked pathway.

REFERENCES

1. **Aharoni, A., C. H. R. de Vos, H. A. Verhoeven, C. A. Maliepaard, G. Kruppa, R. Bino, and D. B. Goodenowe.** 2002. Nontargeted metabolome analysis by use of Fourier transform ion cyclotron mass spectrometry. Omics **6**:217–234.
2. **Bilinski, C. A., I. Russell, and G. G. Stewart.** 1987. Physiological requirements for induction of sporulation in lager yeast. J. Inst. Brew. **92**:216–219.
3. **Cherest, H., and Y. Surdin-Kerjan.** 1978. *S*-Adenosylmethionine requiring mutants in *Saccharomyces cerevisiae*: evidences for the existence of two methionine adenosyl transferases. Mol. Gen. Genet. **163**:153–167.
4. **Donalies, U. E., and U. Stahl.** 2002. Increasing sulphite formation in *Saccharomyces cerevisiae* by overexpression of *MET14* and *SSU1*. Yeast **19**:475–484.
5. **Duan, W., F. A. Roddick, V. J. Higgins, and P. J. Rogers.** 2004. A parallel analysis of H_2S and SO_2 formation by brewing yeast in response to sulfur-containing amino acids and ammonium ions. J. Am. Soc. Brew. Chem. **62**:35–41.
6. **Farfán, M.-J., L. Aparicio, and I. L. Calderón.** 1999. Threonine overproduction in yeast strains carrying the *HOM3-R2* mutant allele under the control of different inducible promoters. Appl. Environ. Microbiol. **65**:110–116.
7. **Fiehn, O., J. Kopka, P. Dörmann, T. Altmann, R. N. Trethewey, and L. Willmitzer.** 2000. Metabolite profiling for plant functional genomics. Nat. Biotechnol. **18**:1157–1161.
8. **Fujii, T., H. Yoshimoto, N. Nagasawa, T. Bogaki, Y. Tamai, and M. Hamachi.** 1996. Nucleotide sequences of alcohol acetyltransferase genes from lager brewing yeast, *Saccharomyces carlsbergensis*. Yeast **12**:593–598.
9. **Gregory, J. C., and J. D. Boeke.** 1996. A useful colony colour phenotype associated with the yeast selectable/counter-selectable marker *MET15*. Yeast **12**:939–941.
10. **Gyllang, H., M. Winge, and C. Korch.** 1989. Regulation of SO_2 formation during fermentation, p. 347–354. *In* European Brewery Convention, Proceedings of the 22nd Congress. Oxford University Press, Oxford, United Kingdom.
11. **Hansen, J., and M. C. Kielland-Brandt.** 1996. Inactivation of *MET10* in brewer's yeast specifically increase SO_2 formation during beer production. Nat. Biotechnol. **14**:1587–1591.
12. **Isnard, A. D., D. Thomas, and Y. Surdin-Kerjan.** 1996. The study of methionine uptake in *Saccharomyces cerevisiae* reveals a new family of amino acid permeases. J. Mol. Biol. **262**:473–484.
13. **Ito, T., T. Chiba, R. Ozawa, M. Yoshida, M. Hattori, and Y. Sakaki.** 2001. Comprehensive two-hybrid analysis to explore the yeast protein interactome. Proc. Natl. Acad. Sci. USA **98**:4569–4574.
14. **Kodama, Y., F. Omura, and T. Ashikari.** 2001. Isolation and characterization of a gene specific to lager brewing yeast that encodes a branched-chain amino acid permease. Appl. Environ. Microbiol. **67**:3455–3462.
15. **Lafaye, A., C. Junot, Y. Pereira, G. Lagniel, J. C. Tabet, E. Ezan, and J. Labarre.** 2005. Combined proteome and metabolite-profiling analyses reveal surprising insights into yeast sulfur metabolism. J. Biol. Chem. **280**: 24723–24730.
16. **Meilhoc, E., J. M. Masson, and J. Teissie.** 1990. High efficiency transformation of intact yeast cells by electric field pulses. Bio/Technology **8**:223–227.
17. **Omura, F., and Y. Shibano.** 1995. Reduction of hydrogen sulfide production in brewing yeast by constitutive expression of *MET25* gene. J. Am. Soc. Brew. Chem. **53**:58–62.
18. **Park, H., and A. T. Bakalinsky.** 2000. *SSU1* mediates sulphite efflux in *Saccharomyces cerevisiae*. Yeast **16**:881–888.
19. **Ramos, C., and I. S. Calderon.** 1992. Overproduction of threonine by *Saccharomyces cerevisiae* mutants resistant to hydroxynorvaline. Appl. Environ. Microbiol. **58**:1677–1682.
20. **Reo, N. V.** 2002. NMR-based metabolomics. Drug Chem. Toxicol. **25**:375–382.
21. **Rose, M. D., F. Winston, and P. Hieter.** 1990. Methods in yeast genetics: a

laboratory course manual. Cold Spring Harbor Laboratory Press, Cold Spring Harbor, NY.
22. **Shimoi, N., H. Fukuda, Y. Fukuda, K. Murata, and A. Kimura.** 1991. Nucleotide sequence and characterization of a gene conferring resistance to ethionine in yeast *Saccharomyces cerevisiae*. J. Ferm. Bioeng. **71**:211–215.
23. **Soga, T., and D. N. Heiger.** 2000. Amino acid analysis by capillary electrophoresis electrospray ionization mass spectrometry. Anal. Chem. **72**:1236–1241.
24. **Soga, T., Y. Ueno, H. Naraoka, Y. Ohashi, M. Tomita, and T. Nishioka.** 2002. Simultaneous determination of anionic intermediates for *Bacillus subtilis* metabolic pathways by capillary electrophoresis electrospray ionization mass spectrometry. Anal. Chem. **74**:2233–2239.
25. **Soga, T., Y. Ohashi, Y. Ueno, H. Naraoka, M. Tomita, and T. Nishioka.** 2003. Quantitative metabolome analysis using capillary electrophoresis mass spectrometry. J. Proteome Res. **2**:488–494.
26. **Takahashi, T., M. Hojito, and K. Sakai.** 1980. Genes controlling hydrogen-sulfide production in *Saccharomyces cerevisiae*. Bull. Brew. Sci. **26**:29–36.
27. **Tamai, Y., K. Tanaka, N. Umemoto, K. Tomizuka, and Y. Kaneko.** 2000. Diversity of the *HO* gene encoding an endonuclease for mating-type conversion in the bottom fermenting yeast *Saccharomyces pastorianus*. Yeast **16**:1335–1343.
28. **Tezuka, H., T. Mori, Y. Okumura, K. Kitabatake, and Y. Tsumura.** 1992. Cloning of a gene suppressing hydrogen sulfide production by *Saccharomyces cerevisiae* and its expression in a brewing yeast. J. Am. Soc. Brew. Chem. **50**:130–133.
29. **Thomas, D., and Y. Surdin-Kerjan.** 1997. Metabolism of sulfur amino acids in *Saccharomyces cerevisiae*. Microbiol. Mol. Biol. Rev. **61**:503–532.
30. **Vaughan-Martini, A., and A. Martini.** 1998. A taxonomic study: Saccharomyces Myen ex Reessm, p. 358–371. *In* C. P. Kurtzman and J. W. Fell (ed.), The yeasts. Elsevier, Amsterdam, The Netherlands.
31. **Wilson, I. D., J. K. Nicholson, J. Castro-Perez, J. H. Granger, K. A. Johnson, B. W. Smith, and R. S. Plumb.** 2005. High resolution "ultra performance" liquid chromatography coupled to oa-TOF mass spectrometry as a tool for differential metabolic pathway profiling in functional genomic studies. J. Proteome Res. **4**:591–598.
32. **Yoshida, S., M. Suzuki, S. Yamano, M. Takeuchi, H. Ikenaga, N. Kioka, H. Sakai, and T. Komano.** 1999. Expression and characterization of rat UDP-*N*-acetylglucosamine: α-3-D-mannnoside β-1,2-*N*-acetylglucosaminyltransferase I in *Saccharomyces cerevisiae*. Glycobiology **9**:53–58.
33. **Yoshida, S., K. Hashimoto, E. Shimada, T. Ishiguro, T. Minato, S. Mizutani, H. Yoshimoto, K. Tashiro, S. Kuhara, and O. Kobayashi.** 2007. Identification of bottom-fermenting yeast genes expressed during lager beer fermentation. Yeast **24**:599–606.
34. **Yoshida, S., K. Hashimoto, K. Kanai-Tanaka, H. Yoshimoto, and O. Kobayashi.** 2007. Identification and characterization amidase-homologous *AMI1* genes of bottom-fermenting yeast. Yeast **24**:1075–1084.

BMC Systems Biology

BioMed Central

Research article

Open Access

Time-resolved metabolomics reveals metabolic modulation in rice foliage

Shigeru Sato[1], Masanori Arita[1,2,3], Tomoyoshi Soga[1,4], Takaaki Nishioka[1,5] and Masaru Tomita*[1,4]

Address: [1]Institute for Advanced Biosciences, Keio University, Tsuruoka, Japan, [2]Department of Computational Biology, Graduate School of Frontier Sciences, The University of Tokyo and PRESTO-JST, Kashiwa, Japan, [3]Plant Science Center, Riken, Yokohama, Japan, [4]Human Metabolome Technologies, Inc., Tsuruoka, Japan and [5]Graduate School of Agriculture, Kyoto University, Kyoto, Japan

Email: Shigeru Sato - n03615ss@sfc.keio.ac.jp; Masanori Arita - arita@k.u-tokyo.ac.jp; Tomoyoshi Soga - soga@sfc.keio.ac.jp; Takaaki Nishioka - takaaki@sfc.keio.ac.jp; Masaru Tomita* - mt@sfc.keio.ac.jp

* Corresponding author

Published: 18 June 2008

BMC Systems Biology 2008, **2**:51 doi:10.1186/1752-0509-2-51

Received: 12 February 2008
Accepted: 18 June 2008

This article is available from: http://www.biomedcentral.com/1752-0509/2/51

© 2008 Sato et al; licensee BioMed Central Ltd.
This is an Open Access article distributed under the terms of the Creative Commons Attribution License (http://creativecommons.org/licenses/by/2.0), which permits unrestricted use, distribution, and reproduction in any medium, provided the original work is properly cited.

Abstract

Background: To elucidate the interaction of dynamics among modules that constitute biological systems, comprehensive datasets obtained from "omics" technologies have been used. In recent plant metabolomics approaches, the reconstruction of metabolic correlation networks has been attempted using statistical techniques. However, the results were unsatisfactory and effective data-mining techniques that apply appropriate comprehensive datasets are needed.

Results: Using capillary electrophoresis mass spectrometry (CE-MS) and capillary electrophoresis diode-array detection (CE-DAD), we analyzed the dynamic changes in the level of 56 basic metabolites in plant foliage (*Oryza sativa* L. ssp. *japonica*) at hourly intervals over a 24-hr period. Unsupervised clustering of comprehensive metabolic profiles using Kohonen's self-organizing map (SOM) allowed classification of the biochemical pathways activated by the light and dark cycle. The carbon and nitrogen (C/N) metabolism in both periods was also visualized as a phenotypic linkage map that connects network modules on the basis of traditional metabolic pathways rather than pairwise correlations among metabolites. The regulatory networks of C/N assimilation/dissimilation at each time point were consistent with previous works on plant metabolism. In response to environmental stress, glutathione and spermidine fluctuated synchronously with their regulatory targets. Adenine nucleosides and nicotinamide coenzymes were regulated by phosphorylation and dephosphorylation. We also demonstrated that SOM analysis was applicable to the estimation of unidentifiable metabolites in metabolome analysis. Hierarchical clustering of a correlation coefficient matrix could help identify the bottleneck enzymes that regulate metabolic networks.

Conclusion: Our results showed that our SOM analysis with appropriate metabolic time-courses effectively revealed the synchronous dynamics among metabolic modules and elucidated the underlying biochemical functions. The application of discrimination of unidentified metabolites and the identification of bottleneck enzymatic steps even to non-targeted comprehensive analysis promise to facilitate an understanding of large-scale interactions among components in biological systems.

Background

In the post-genome era, comprehensive data from "omics" technologies (genomics, transcriptomics, proteomics, and metabolomics) have been extensively analyzed to elucidate the underlying biochemical networks that elaborately regulate cellular mechanisms. Recent contributions from metabolomics are particularly noteworthy; they offer insights into metabolism that complement information obtained from proteomics and transcriptomics [1]. Correlation analysis of metabolic profiles has been used effectively to distinguish silent phenotypes or genetic alterations that are not noticeable superficially [2-4]. The systematic integration of metabolomic-, proteomic-, and transcriptomic profiles facilitates the unbiased, information-based reconstruction of underlying biochemical networks [5,6]. Kohonen's self-organizing map (SOM) analysis [7] was also an effective method to classify and monitor metabolic alteration patterns with time-series profiles [8,9].

However, with the current technology, unbiased reconstruction from comprehensive and high-throughput data is challenging; statistical tools are immature and inherent measurement errors and biological noise continue to present problems [10]. Moreover, two issues are relevant to the exploitation of metabolomics data. First, it is crucial to interpret metabolic profiles by focusing on a specific rhythm in an appropriate time range and interval, since plants have adapted their metabolism to different environmental fluctuations such as the slow and steady diurnal rhythm, whereas metabolic levels change dynamically. Second, currently available metabolomics data are insufficient for the detection of new metabolic networks. Even if non-target profiling were able to quantify thousands of metabolites, at present there is no method for estimating their reliability. As statistical inference requires large amounts of data measured under similar conditions in transcriptomics [11], the verification of network dynamics for known pathways must precede attempts to identify unknown network structures. It appears that each metabolic profile is measured under method-specific, presumably biased conditions.

Time-resolved target analysis is an effective way to observe biochemical dynamics. We systematically measured the level of 56 basic metabolites in rice leaves (*Oryza sativa* L. ssp. *japonica*) at hourly intervals over a 24-hr period. Our target and experimental conditions were strategically determined: 1) we focused on primary metabolic pathways consisting of carbon fixation/respiration- and nitrogen assimilation/dissimilation pathways, and comprehensively quantified related metabolites, 2) the photocycle was the sole environmental factor, and 3) measurements were made at 1-hr intervals to allow the observation of dynamic profiles.

High-throughput analysis was conducted with the capillary electrophoresis – mass spectrometry (CE-MS) technology we developed earlier [12-14], and has been applied to metabolic profiling in *Bacillus subtilis* extracts [15] and monitoring of genetic and environmental perturbations in *Escherichia coli* cells [16]. Each employed CE-MS method was able to detect charged low molecular metabolites in less than 30 min without requiring derivatization. Combined with diode array detection (CE-DAD), our technology is also applicable to quantifying small sugar compounds. We previously developed a sample preparation protocol that could extract metabolites with possibly minimal metabolic turnover [17]. By using the CE-MS and CE-DAD, we also succeeded in analyzing over eighty major metabolites (sugars, organic acids, amino acids, and nucleotides) in rice foliage. The current work is our first systematic time-course measurements of rice foliage throughout a day.

We applied four information-based methods to analyze the diurnal fluctuation of metabolites: 1) metabolic pathways were classified with SOM to monitor the metabolic dynamics in each time-step, 2) a phenotypic linkage map was constructed from the classified pathways by Sammon's 2D-network layout [18], 3) unidentified metabolites were predicted based on SOM analysis and chemical structures, and 4) rate-limiting enzymes were identified by hierarchical clustering on a correlation matrix. Here we show that combining metabolome analysis and information-based methods is an effective way to elucidate phenotypical metabolic network structures and underlying biological functions under diurnal rhythm fluctuations.

Results

Time-course data acquisition

We extracted target metabolites existing in the primary metabolism such as the glycolytic pathway, the reductive- and oxidative pentose phosphate pathway, and the photorespiratory pathway, the tricarboxylic acid (TCA) cycle, and the amino acid biosynthetic pathway. Figure 1 presents the practical rice biochemical network that was constructed with our target metabolites based on annotated protein data from the KEGG pathway database [19], Swiss-Prot database [20], or Rice Annotation Project Data Base [21]. It shows the names of target metabolites and the EC number of enzymatic reactions; black dots are non-target metabolites. Although NH_3 (also R-NH_2) and CO_2 were non-target compounds, they are shown in green to demonstrate in and out of carbon and nitrogen.

We selected eight enzymatic proteins that have not been annotated at this stage to determine whether they function in the rice plant. These enzymes and the judgment criteria are shown in Table 1. On the map, their EC numbers and lines are presented in gray.

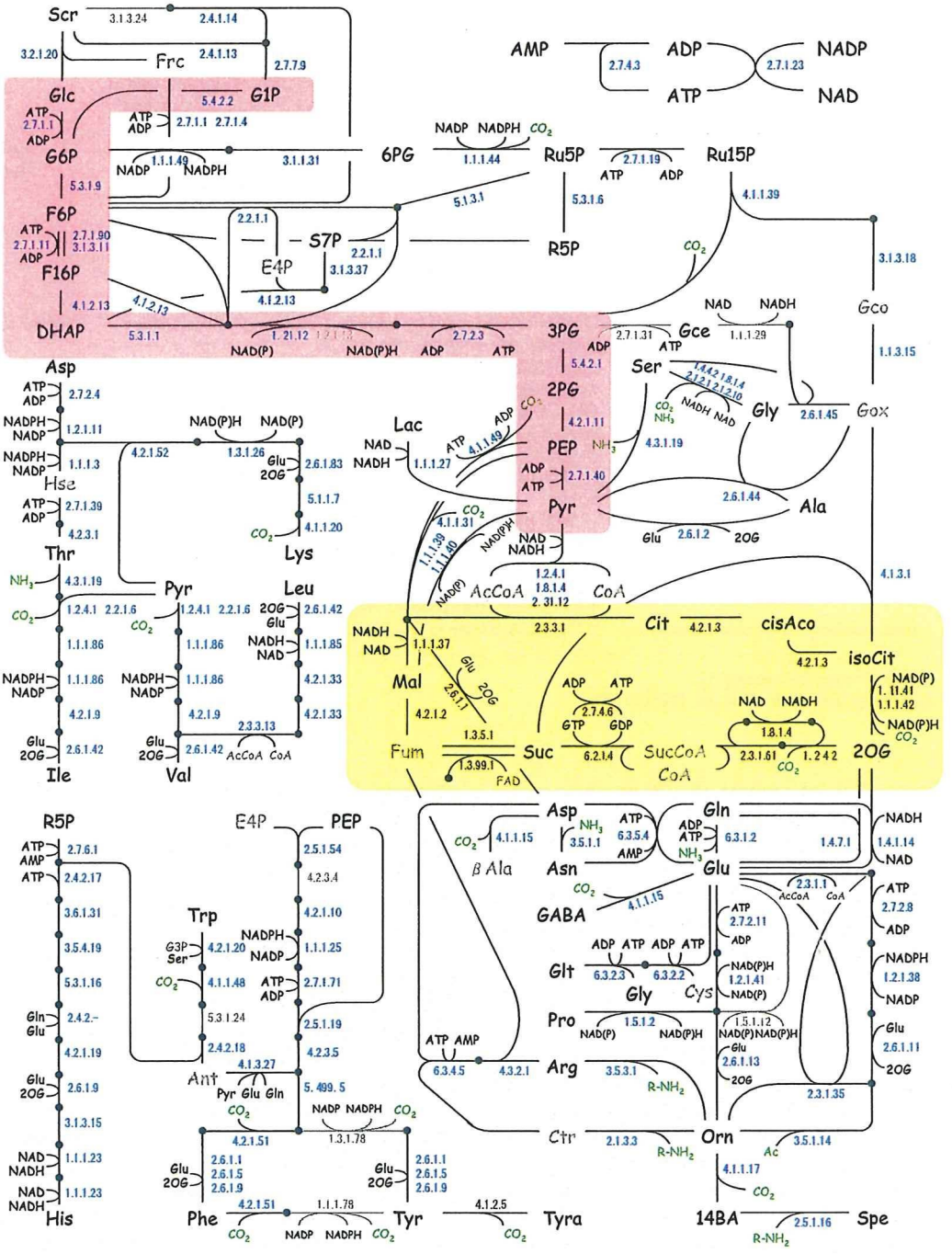

Figure 1

Metabolic network of *oryza sativa* L. ssp. *Japonica*. Target metabolites and practical enzymatic reactions are shown. The number next to the line is the EC number. Colors indicate the ratio of metabolic levels in light and dark periods. Unidentified metabolites are gray and gray lines and EC numbers identify non-annotated enzymatic proteins. The red- and yellow shade show the glycolytic pathway and the TCA cycle respectively.

Table 1: Selected non-annotated proteins expected to function in rice plant

EC Number	Enzyme name	Criterion for judgement	Ref.
1.1.1.29	hydroxypyruvate reductase; glycerate dehydrogenase	Enzymatic reduction of hydroxypyruvic acid to D-glyceric acid in higher plants, i.e. the leaves of pea, beet, tomato, radish, spinach, parsley, lettuce, corn, kohlrabi, and carrot.	[22]
		AK069655; Similar to 2-hydroxyacid dehydrogenase	RAP-DB*1
1.2.1.13	glyceraldehyde-3-phosphate dehydrogenase	AK071685; Similar to GADPH (383AA) (Fragment). AK67755; Similar to Glyceraldehyde-3-phosphate dehydrogenase (EC 1.2.1.13) (Fragment).	RAP-DB
1.3.1.78	arogenate dehydrogenase; prehenate dehydrogenase	TyrAAT1(AF434681) and TyrAAT2(AF434682) in *Arabidopsis thaliana* catalyze the oxidative decarboxylation of arogenate into Tyr in the presence of NADP. TyrAAT also exhibits prephenate dehydrogenase activity.	[23]
		Q5Z9H5_ORYSJ; Q5Z9H3_ORYSJ; Q5Z6Y1_ORYSJ, Putative arogenate dehydrogenase isoform 2	Swiss-Prot/TrEMBL*2
1.5.1.12	delta-1-pyrroline-5-carboxylate dehydrogenase	AK121765; Similar to delta-1-pyrroline-5-carbozylate dehydrogenase	RAP-DB
2.7.1.31	D-glycerate 3-kinase	GLYK family protein was purified and sequenced from *Arabidopsis thaliana*, identified as putative kinase-annotated single-copy gene At1g8038. This article suggests that an *Olyza sativa* PRK/UK-like protein, BAD73764, Os01g48990 is grouped with the GLYK kinase family.	[24]
3.1.3.24	sucrose-phosphatase	AK063330, AK071525, AK064563; Similar to sucrose-phosphatase	RAP-DB
4.2.3.4	3-dehydroquinate synthase	Pentafunctional aroma enzyme in Saccharomyces cervisiae includes EC 4.2.3.4, EC 4.2.1.10, EC 2.5.1.19, EC 1.1.1.25, and EC 2.7.1.71.	[25]
		AK071977; Similar to 3-dehydroquinate synthase-like protein (EC 4.2.3.4). Four other proteins were annotated.	RAP-DB
5.3.1.24	phosphoribosyl-anthranilate isomerase	J075072K08; Similar to phosphoribosylanthranilate isomerase	RAP-DB

*1: Rice Annotation Project Data Base [21]
*2: UniProt Knowledge base: Swiss-Plot and TrEMBL [20]

Sedoheptulose 1,7-bisphosphate (S17P) in the pentose phosphate pathway was not identified because the standard reagent was unavailable. Xylulose 5-phosphate (X5P) is a stereoisomer of Ribulose 5-phosphate (Ru5P) and their peak overlap in CE-MS analysis makes the identification even more difficult. Glyceraldehyde 3-phosphate (G3P) and oxaloacetate (OAA) were not accurately determined too, because they were readily reacted or decomposed.

The seventy selected target metabolites were classified into four groups according to their chemical structure-based physiochemical characteristics (Table 2). Group A contained amino acids and amines, group B organic acids and sugar phosphates, group C nucleotides and coenzymes, and group D sugars. Groups A, B, and C, consisting of ionic substances, were analyzed with three CE-MS methods for cationic, anionic, and nucleotide metabolites; analysis of group D was with a CE-DAD method. For CE separation, we used conventional sample preparation with simple and universal procedures without any derivatization process. As common preparation procedures were applicable under the four analytical conditions, we were able to determine simultaneously a wide variety of chemical compounds.

Plant seedlings were grown under a 13-hr light – 11-hr dark photocycle for 20 to 21 days. The level of the 56 metabolites was successfully quantified at hourly intervals over the course of 24 hr. We could identify the peak and determine the peak area for S7P but could not quantify its level, since the reagent was not available at the time of our CE-MS measurement; we later qualitatively identified its peak with the migration time ratio (MT/MT_{IS}) of S7P to PIPES (internal standard). The other 13 metabolites were under the detection limit (signal-to-noise ratio (S/N) < 3); their names were colored gray in Figure 1.

In the course of 24 hr, the metabolites exhibited various fluctuations (Figure 2). Ru15P, the precursor of carbon fixation, manifested a variation synchronous with the photoperiod; its intracellular concentration increased under illumination and decreased in darkness. Several metabolites exhibited similar light-dependent variations in the reductive pentose phosphate pathway (3PG, R5P, and Ru5P), the glycolytic pathway (3PG, 2PG, PEP, Pyr), the TCA cycle (2OG, Suc, and Mal), and in sugars (Scr and Glc). Citrate, on the other hand, manifested opposite fluctuation changes. In the amino acid biosynthesis pathway, major amino acids (Ala, Asn, Gln, Glu, Gly, and Ser) accumulated during the light period. Minor amino acids that

Table 2: The 70 target metabolites subjected to analysis of time-resolved dynamics and their abbreviation used in this article

Group A (CE-MS No.1)		Group B (CE-MS No.2)		Group C (CE-MS No.3)	
Amino acids		***Organic acids***		***Nucleotides***	
Ala	Alanine	*cis*Aco	*cis*-Aconitate	AMP	AMP
βAla	β-Alanine	Cit	Citrate	ADP	ADP
GABA	γ-Aminobutyrate	*iso*Cit	*iso*-Citrate	ATP	ATP
Ant	Anthranilate	DHAP	Dihydroxyacetonephosphate	GDP	GDP
Arg	Arginine	Fum	Fumarate	GTP	GTP
Asn	Asparagine	Gce	Glycerate	***Coenzymes***	
Asp	Aspartate	Gco	Glycolate	NAD	NAD
Ctr	Citrulline	Gox	Glyoxylate	NADH	NADH
Cys	Cysteine	Lac	Lactate	NADP	NADP
Glu	Glutamate	Mal	Malate	NADPH	NADPH
Gln	Glutamine	2OG	2-Oxoglutarate	CoA	CoA
Glt	Glutathione red.	PEP	Phospho*enol*pyruvate	AcCoA	Acetyl-CoA
Gly	Glycine	6PG	6-Phosphogluconate	SucCoA	Succinyl-CoA
His	Histidine	2PG	2-Phosphoglycerate		
Hse	Homoserine	3PG	3-Phosphoglycerate		
Leu	Leucine	Pyr	Pyruvate	Group D (CE-DAD)	
Ile	*iso*-Leucine	Suc	Succinate	***Sugars***	
Lys	Lysine	***Sugar Phosphate***		Frc	Fructose
Orn	Ornithine	E4P	Erythrose 4-phosphate	Glu	Glucose
Phe	Phenylalanine	F16P	Fructose 1,6-bisphosphate	Suc	Sucrose
Pro	Proline	F6P	Fructose 6-phosphate		
Ser	Serine	G1P	Glucose 1-phosphate		
Thr	Threonine	G6P	Glucose 6-phosphate		
Trp	Tryptophan	R5P	Ribose 5-phosphate		
Tyr	Tyrosine	Ru15P	Ribulose 1,5-bisphosphate		
Val	Valine	Ru5P	Ribulose 5-phosphate		
Amines		S7P	Sedoheptulose 7-ohosphate		
14BA	1,4-Butanediamine				
Spe	Spermidine				
Tyra	Tyramine				

are synthesized from specific organic acids through several reaction steps (His, Ile, Leu, Lys, Phe, Trp and Val) accumulated during the dark period.

Table 3 shows the status of adenine nucleosides and nicotinamide coenzymes in the light and dark periods. Whereas the ratios of ADP, NADP, and NADH were almost equal in the light and dark periods, the ratios of AMP and NADPH were higher and those of ATP and NAD were lower in the light period (see Discussion).

Self-organizing map and phenotypic linkage of metabolic modules

To visualize the functioning networks throughout a 24-hr period, we classified the metabolites according to similarities in their time-dependent behavior by using Kohonen's self-organizing map (SOM) and Sammon's 2D-network layout (Sammon map). The time-dependent levels of each metabolite were represented as a 24-dimensional vector. On the SOM, the 57 metabolites were classified into a 24 × 24 lattice on the basis of vector similarity. The map was roughly divided into two major groups (see the dark gray line in Figure 3A). Metabolites with high levels in the light period are in the left area; those with high levels in the dark period are on the right in the map. On the SOM, each group was further classified and assigned to subgroups consisting of nitrogen- and carbon-assimilating compounds. Certain amino acids were arranged near their precursor organic acids, e.g., Glu/2OG. Gly, Ser, and Ala were grouped with synthetic pathway intermediates such as Pyr and Gce. The degree of similarity among metabolites was quantitatively visualized on the Sammon map; it shows approximate distances between metabolites on the SOM according to the Euclidean distance of the input vectors (Figure 3B). When we merged neighboring metabolites on the Sammon map we obtained 12 subsets of metabolites. Each subset is composed of metabolites that exhibit synchronous, time-dependent fluctuations, a "metabolic module". Metabolites in the same module were often neighbors in a traditional metabolic pathway network. Products that accumulated during the light period were arranged in subsets M1 – M8. They included the module for the reductive pentose phosphate pathway (M3), the photorespiratory pathway (M2), the latter half of the gly-